

**PROPOSAL TO CONTINUE THE STUDY OF  
CHARMONIUM SPECTROSCOPY IN  
PROTON-ANTIPROTON ANNIHILATIONS**

**(Revised proposal P-835)**

T.A. Armstrong<sup>6</sup>, D. Bettoni<sup>2</sup>, V. Bharadwaj<sup>1</sup>, C. Biino<sup>7</sup>, G. Borreani<sup>7</sup>, D. Broemmelsiek<sup>4,\*</sup>, A. Buzzo<sup>3</sup>, R. Calabrese<sup>2</sup>, A. Ceccucci<sup>7</sup>, R. Cester<sup>7</sup>, M. Church<sup>1</sup>, P. Dalpiaz<sup>2</sup>, P.F. Dalpiaz<sup>2</sup>, D. Dimitroyannis<sup>5</sup>, M. Fabbri<sup>2</sup>, J. Fast<sup>4,\*</sup>, A. Gianoli<sup>2</sup>, C.M. Ginsburg<sup>5,\*</sup>, K. Gollwitzer<sup>4,\*</sup>, A. Hahn<sup>1</sup>, M. Hasan<sup>6</sup>, S. Hsueh<sup>1</sup>, R. Lewis<sup>6</sup>, M. Lovetere<sup>3</sup>, E. Luppi<sup>2</sup>, M. Macri<sup>3</sup>, A.M. Majewska<sup>6,\*</sup>, M. Mandelkern<sup>4</sup>, F. Marchetto<sup>7</sup>, M. Marinelli<sup>3</sup>, J. Marques<sup>4,\*</sup>, W. Marsh<sup>1</sup>, M. Martini<sup>2</sup>, M. Masuzawa<sup>5,\*</sup>, E. Menichetti<sup>7</sup>, A. Migliori<sup>7</sup>, R. Mussa<sup>7</sup>, M. Pallavicini<sup>3</sup>, S. Palestini<sup>7</sup>, S. Passaggio<sup>3</sup>, N. Pastrone<sup>7</sup>, C. Patrignani<sup>3</sup>, J. Peoples Jr.<sup>1</sup>, F. Petrucci<sup>2</sup>, M.G. Pia<sup>3</sup>, S. Pordes<sup>1</sup>, P. Rapidis<sup>1</sup>, R. Ray<sup>1</sup>, J. Reid<sup>6,\*</sup>, G. Rinaudo<sup>7</sup>, B. Rocuzzo<sup>7</sup>, J. Rosen<sup>5</sup>, A. Santroni<sup>3</sup>, M. Sarmiento<sup>5</sup>, M. Savrie<sup>2</sup>, J. Schultz<sup>4</sup>, K.K. Seth<sup>5</sup>, A. Smith<sup>4,\*</sup>, G.A. Smith<sup>6</sup>, M. Sozzi<sup>7</sup>, S. Trokenheim<sup>5,\*</sup>, S. Werkema<sup>1</sup>, Y. Zhang<sup>6</sup>, J. Zhao<sup>5,\*</sup>, G. Zioulas<sup>4</sup>.

<sup>1</sup> *Fermi National Accelerator Laboratory, Batavia, Illinois 60510, U.S.A.*

<sup>2</sup> *I.N.F.N. and University of Ferrara, 44100 Ferrara, Italy*

<sup>3</sup> *I.N.F.N. and University of Genoa, 16146 Genoa, Italy*

<sup>4</sup> *University of California at Irvine, California 92717, U.S.A.*

<sup>5</sup> *Northwestern University, Evanston, Illinois 60208, U.S.A.*

<sup>6</sup> *Pennsylvania State University, University Park, Pennsylvania 16802, U.S.A.*

<sup>7</sup> *I.N.F.N. and University of Turin, 10125 Turin, Italy.*

\* *Student expected to graduate on current data.*

**The E760 Collaboration**

September 1 1992

## 1. Introduction

In the fall of 1990 we submitted a proposal [1] to extend the data taking of E760 to the next fixed target period, now scheduled to start in the fall of 1994, in order to complete the study of the masses, widths and branching fractions of charmonium states and to extend the program to include a search for cryptoexotics and a study of  $J/\psi$  formation in nuclear matter.

During the five month data taking period in 1991 we have obtained not only significant physics results but acquired a better understanding of what is needed in order to complete our study of charmonium states. In spite of the fact that we have collected data for an integrated luminosity ( $30pb^{-1}$ ) which was in excess of what we had hoped for, we achieved only part of our goals. If we compare the estimates given in the previous version of this proposal to the actual experimental situation, (see Table 12 in the Appendix) we find that, in general, the expected cross sections were overestimated and while the measured background levels and efficiencies are close to prediction for channels with a large mass  $e^+e^-$  in the final state, they compare unfavorably with the predictions for neutral final states. In the light of the results obtained during the 1991 run it is therefore mandatory to review our program giving new estimates for the required luminosities and restating the priority we assign to each measurement.

In section 2 we discuss the measurements of highest priority :

- a) determination of mass and total width of the  $\eta_c$  and of the product of the branching fractions  $B(\eta_c \rightarrow \bar{p}p) \times B(\eta_c \rightarrow \gamma\gamma)$
- b) confirmation of the  $^1P_1$  signal and a more precise determination of the  $^1P_1$  parameters
- c) search for the  $\eta'_c$  and determination of its mass and width
- d) determination of the mass and total width of the  $\chi_0$  and of the products of the branching fractions  $B(\chi_0 \rightarrow \bar{p}p) \times B(\chi_0 \rightarrow \gamma\gamma)$  and of  $B(\chi_0 \rightarrow \bar{p}p) \times B(\chi_0 \rightarrow J/\psi + \gamma)$

Since we shall spend some calibration time at the well-measured resonances, we also discuss

a measurement of the angular distributions in radiative decays of the  $\chi_1$  and  $\chi_2$ .

In section 3 we discuss the feasibility of a search for the missing D-states of charmonium. The discovery of these states is very important but the uncertainties on mass values and formation/decay branching fractions make this measurement risky. For this reason we will not begin this search until the measurements described above are successfully completed.

Section 4 gives a description of measurements which are unrelated to charmonium physics but are of considerable interest and can be done concurrently with the measurements on charmonium states.

According to the new estimates, the program outlined will not be completed in the next fixed target run unless we substantially increase the instantaneous luminosity of the experiment. This will be possible with the expected increase in stacking rate of the Antiproton source and with an upgrade of the hydrogen gas-jet target system. A description of the planned modifications to the target and of the implications of running with high currents in the Antiproton Accumulator is given in section 5.

Section 6 contains a description of the detector upgrades needed to cope with the increased instantaneous rates.

Finally in section 7 we discuss other measurements to which we do not attach high priority but which could be performed with some extra running time. These include the study of  $\bar{p}p \rightarrow \eta_c \rightarrow \phi\phi$  and the measurement of  $J/\psi$  - nucleon cross section.

## **2. Measurement of the parameters of $\eta_c$ , $^1P_1$ , $\chi_0$ and search for the $\eta'_c$**

### **Measurement of the line parameters of the $\eta_c$**

Fig.1 shows the excitation curve for the reaction  $\bar{p}p \rightarrow \eta_c \rightarrow \gamma\gamma$  obtained in 1991 with an integrated luminosity of  $\sim 3.6pb^{-1}$ . The acceptance $\times$ efficiency factor is only 0.13 since to

reject the large background we are forced to restrict the acceptance to  $|\cos \theta_{cm}| \leq 0.2$ . A large (and unanticipated) component of the background comes from the process  $\bar{p}p \rightarrow \pi^0 + \gamma$ . If we fit this data to a Breit-Wigner plus a background we determine a total width  $\Gamma_{Tot} = (20 \pm 10)$  MeV and, using the current value [2] for  $B(\eta_c \rightarrow \bar{p}p) = (1.2 \pm 0.4) \times 10^{-3}$ , we extract from the product of branching ratios to the initial and final states,  $B(\eta_c \rightarrow \gamma\gamma) = (3.3 \pm 1.4) \times 10^{-4}$  (preliminary). This branching fraction gives in good approximation the ratio  $\frac{\Gamma(\eta_c \rightarrow \gamma\gamma)}{\Gamma(\eta_c \rightarrow \text{light hadrons})}$ , a quantity from which the value of the strong coupling constant at the mass of the c-quark  $\alpha_s(m_c)$  can be directly derived[3]. We notice that this measurement represents already a substantial improvement on existing ones [2], however the result depends on the value of the branching fraction to  $\bar{p}p$  measured by other experiments. A precise measurement of the total width and of the product of branching ratios to the initial and final states, coupled with the measurement of the partial width to  $\gamma\gamma$  at  $e^+e^-$  colliders would provide enough information to check the internal consistency of all these measurements. We have estimated that, with the same background rejection as obtained in the past run, we need  $\sim 20 \text{ pb}^{-1}$  of total integrated luminosity to obtain a 25% measurement of the total width and a 15% measurement of the product of branching ratios. Precise measurements of the parameters of the  $\eta_c$  are a milestone essential for planning and understanding the measurements described in the next two subsections.

### Study of the $^1P_1$

Precise measurements of the parameters which characterize the  $h_c(^1P_1)$  state are useful to resolve a number of open questions in heavy quark physics. The value of the hyperfine splitting of P states is a sensitive probe of the deviation from a  $\frac{1}{r}$  dependence of the vector part of the potential[4]. A measurement of the total width and of the partial width to  $\eta_c + \gamma$  will provide an estimate of the partial width to gluons. Since calculations of partial gluonic widths of  $^{1,3}P_1$  states suffer from infrared divergences to leading order, a comparison with measured values will be of guidance. Calculations of branching ratios for hadronic decays to lower ( $\bar{c}c$ ) states also give contradictory answers and the debate could profit from some actual data[5].

Ours is apparently the only experiment which can at present study the  $^1P_1$  state of charmonium. However it will be hard to obtain enough data to resolve all the issues mentioned above. Fig. 2 shows the rate versus center of mass energy for the reaction  $\bar{p}p \rightarrow J/\psi + \pi^0$  measured in 1991 with an integrated luminosity of  $\sim 16pb^{-1}$  [6]. A careful analysis of the statistical significance of the structure observed in Fig. 2 shows that the probability that a signal of magnitude equal to or greater than the one observed could originate from a fluctuation of the continuum anywhere in the scanned interval is 1 in 400. We clearly must repeat the scan with higher statistics. In the 1991 run we have measured the  $^1P_1$  mass to be  $3526.2 \pm 0.15 \pm 0.2 \text{ MeV}/c^2$  but could only set an upper limit of 1.1 MeV (90% C.L.) to its width. We estimate the luminosity to perform a 30% measurement of the width in the hypothesis that it is in the range from 0.6 to 1.0 MeV, to be  $75pb^{-1}$ . For this measurement it is essential that the beam width be  $\simeq 300keV$ . It will be important to detect other decay channels; we have found no events from the decay  $^1P_1 \rightarrow J/\psi\pi\pi$  and set a limit of  $\leq 0.18$  (90% C.L.) to the ratio  $\frac{^1P_1 \rightarrow J/\psi\pi\pi}{^1P_1 \rightarrow J/\psi\pi^0}$ . The most pessimistic prediction for this ratio[5] is  $\sim 0.05$  and therefore, in a  $75pb^{-1}$  run we should expect to see some events in this background free channel. As for the decay channel  $^1P_1 \rightarrow \eta_c + \gamma$ , unfortunately in our experiment we can only see the  $\eta_c$  through its decay to  $\gamma\gamma$  which, as mentioned above, has a branching fraction of  $(3.4 \pm 1.1) \times 10^{-4}$ . \* If the branching fraction for  $^1P_1 \rightarrow \eta_c + \gamma$  is  $\sim 50\%$  we expect the signal in the  $3\gamma$  final state to show up at approximately the same level as the  $(e^+e^-)_{J/\psi} + \pi^0$  signal. However in this case the background, which comes from incompletely observed neutral final states, is much higher than for the  $(e^+e^-)_{J/\psi} + \pi^0$  channel. The present data sample does not show evidence for this decay mode. In order to extract this signal it will be important not only to increase substantially the data sample but also to reject the background more efficiently. The background to  $3\gamma$  events comes predominantly from neutral final states with

---

\*Consideration is being given to the feasibility of studying the reaction:  $\bar{p}p \rightarrow ^1P_1 \rightarrow \eta_c\gamma \rightarrow \phi\phi\gamma \rightarrow 2K^+2K^-\gamma$ . The background comes mainly from four charged particles plus  $\pi^0$ . The fraction of  $\pi^0$ 's that would give only one photon above 50 MeV in the acceptance and survive all the remaining selections is 1/30. This and the absence of a  $\phi\phi\gamma$  continuum background are the factors that might make this channel accessible in spite of the small cross section.

three  $\pi^0$ 's where three of the  $\gamma$ 's escape detection either because they have energy below the calorimeter detection threshold or because they fall outside the acceptance. The two ways of reducing the backgrounds are then obviously to increase the detector acceptance and to lower the threshold, and we propose to pursue them both. We postpone to section 6 a detailed discussion of how we plan to use the existing detector more effectively. To increase the acceptance we propose to build a compact calorimeter (see Fig. 3) to cover the polar angle range from  $70^\circ$  to  $140^\circ$  and 75% of the full azimuthal range. There are many advantages in adding this detector: an important one is the possibility of extending the angular acceptance for events with a large mass electron pair in the final state. We have calculated that by increasing the acceptance for the electron tracks from the present polar angle fiducial range ( $15^\circ \leq \theta \leq 60^\circ$ ) to the range  $5^\circ \leq \theta \leq 110^\circ$  we would increase the geometrical acceptance by a factor 2 even accounting for the 75% coverage in azimuth at large angles. The advantage would not only be that of reducing the luminosity requirements but also of substantially improving angular distribution measurements. Using the information available in our present data we are now trying to establish if it will be possible to trigger and extract a low level signal for this new type of events.

### Search for the $\eta'_c$

The only evidence for the  $\eta'_c$  comes from an early experiment at SPEAR [7] which measured a mass difference of  $\sim 90$  MeV between the  $\eta'_c$  and the  $\psi'$ . This large difference is hard to reconcile with theoretical predictions unless coupled channel effects are large. It is important to confirm the result of the SPEAR experiment and to measure accurately the mass and total width of the  $\eta'_c$  and the product of its branching ratios to the initial ( $\bar{p}p$ ) state and to the  $\gamma\gamma$  final state. E760 started but, for lack of running time, did not complete a search for the  $\eta'_c$ . Fig. 4 shows the result of the scan done at center of mass energies above 3.5 GeV searching for  $\gamma\gamma$  final states. The only high point is at the  $\chi_2$  where we see a  $\sim 4\sigma$  signal[8]. We now compare the observed  $\sim 11pb$  background cross section level with what we expect for the  $\eta'_c$  signal. In this estimate we take the branching fraction to  $\gamma\gamma$  to be the same as for the  $\eta_c$ , and the branching fraction to  $\bar{p}p$  to scale as  $M_R^{-8}$ [9]. Using as an input value the

peak cross section measured by E760 for the  $\eta_c$  we obtain  $\sigma_{peak}(\eta'_c) \approx 47 pb$  which must be reduced by an efficiency  $\times$  acceptance factor  $\sim 0.71 \times 0.4$  to  $13 pb$ . If the assumptions made in the calculation are correct, we should have seen a cross-section jump comparable to that seen at the  $\chi_2$  if, in our scan, we had landed on the peak of the  $\eta'_c$  resonance. It is clear that no conclusion can be drawn at this time from the data taken in 1991, and that we will need some luck to spot this state quickly in the next run. From the existing information, the best guess is that the  $\eta'_c$  width is about 7 MeV. A possible scan strategy could then be the following: maximum range covered  $\sqrt{s} = 3585 MeV$  to  $\sqrt{s} = 3646 MeV$ , step size 2.5 MeV, luminosity/point  $1.5 pb^{-1}$ . Start at the lower end to check the SPEAR result. Assuming the background is known (certainly true after the first few points) a point at the peak would give us a  $3\sigma$  enhancement. The scan over the full range would cost us approximately  $35 pb^{-1}$ . Once the resonance is found we will need only  $10 pb^{-1}$  to measure its width to 20% and the product of the branching ratios to the initial and final state to 15%. This calculation assumes that the background level is the same as in the past run. However the improvements in the calorimeter readout and the addition of a new detector at large angles may reduce substantially the main background component which, at these energies, comes from  $2\pi^0$  final states where one of the photons either falls outside the acceptance or is below the energy detection threshold.

### Measurement of the line parameters of the $\chi_0$

Recently the study of P-state annihilations into two photons and two gluons has received much attention and calculations involving relativistic corrections [10] and new factorization schemes [11] have been performed. E760 has obtained new precise results for the total width of the  $\chi_1$  and  $\chi_2$  [12] and for the partial width to  $\gamma\gamma$  of the  $\chi_2$  [8]. Similar quality measurements on the  $\chi_0$  will complete our knowledge of  $^3P$  states and provide stringent tests of the theoretical predictions. We note that perturbative QCD calculations directly relate  $^3P_2$  and  $^3P_0$  states and not the  $^3P_1$  state. The mass of the  $\chi_0$  has been measured with sufficient accuracy at SPEAR ( $M(\chi_0) = (3415.1 \pm 1.0) MeV/c^2$ ) [7] to allow for an efficient scan. To estimate the amount of luminosity needed to perform a good measurement of the total

width we assume that the branching ratio to  $\bar{p}p$  is close to that measured for the  $\chi_1$  and the  $\chi_2$ ,  $\sim .8 \times 10^{-4}$ . We will study two decay channels  $\chi_0 \rightarrow J/\psi + \gamma$  and  $\chi_0 \rightarrow \gamma\gamma$ . The first branching ratio has been measured reasonably well  $((6.6 \pm 1.8) \times 10^{-3})$  and the second only approximately  $((4.0 \pm 2.3) \times 10^{-4})$ . Using these values we find that the luminosity needed for a 30% measurement of the  $\chi_0$  width is  $\sim 20 pb^{-1}$ . At the same time we will measure to 15% the product of the branching ratio to  $\bar{p}p$  and the branching ratio to  $J/\psi + \gamma$  and of the ratio  $\frac{\chi_0 \rightarrow \gamma\gamma}{\chi_0 \rightarrow J/\psi + \gamma}$ .

In Table 1 we summarize the luminosity requirements and the precision expected in the measurements for each resonance.

Table 1:

Decay channel	luminosity requirement $pb^{-1}$	% error on $\Gamma_{tot}$	% error on $Br_{in} \times Br_{out}$
$^1P_1 \rightarrow J/\psi + \pi^0$	75	30	30
$\eta'_c \rightarrow \gamma\gamma$	45	20	15
$\eta_c \rightarrow \gamma\gamma$	20	25	15
$\chi_0 \rightarrow J/\psi + \gamma$	20	25	20
<b>Total</b>	160		

### Angular distributions in radiative decays of $\chi_1$ and $\chi_2$ .

During the 1990 and 1991 running periods we have collected about 3000  $\chi_2$  events and 400  $\chi_1$  events in the reaction  $\bar{p}p \rightarrow \chi_J \rightarrow J/\psi \gamma \rightarrow e^+e^-\gamma$ . Using those events we have measured  $a_2$  (the quadrupole amplitude in the radiative decay) with an accuracy of 0.06 for both  $\chi_2$  and  $\chi_1$ .

The measurement of  $a_2(\chi_2)$  is already the most accurate in the world. This is not the case for  $\chi_1$ , where there exists a more accurate measurement done by the Crystal Ball collaboration [13]. In order to achieve their accuracy ( $\pm 0.02$ ) we would have to increase our statistics by a factor of 8.5, which would require approximately  $3.3 pb^{-1}$  of integrated

luminosity.

It is important to measure both angular distributions to the same accuracy in the same experiment and compare the ratio  $\frac{a_2(\chi_2)}{a_2(\chi_1)}$  with the value of  $3/\sqrt{5}$  predicted by theory [14]. This prediction is not affected by uncertainties in the values of the quark mass and anomalous magnetic moment.

### 3. The Search for the Spin 2 Charmonium $D$ States

The charmonium  $D$  states are a poorly studied sector of heavy quark physics. The  $J=2$   $D$  states ought to be extremely narrow despite being above the open charm threshold. Their annihilation and radiative decays provide an interesting test of QCD.

The charmonium  $D$  state which has been observed is the  $\psi(3770)$ , generally considered to be largely triplet  $D_1$  with a small admixture of the  $n=2$  triplet  $S_1$ . Its decay is dominated by the  $\bar{D}D$  mode. Measured partial widths are:  $e^+e^-$  (0.26 keV),  $J/\psi\pi\pi$  (50 keV), light hadrons [ggg+virtual gamma] (300 keV), and E1 radiative decay to  $\chi_0$  and  $\chi_1$  (500 keV and 440 keV respectively). The triplet  $D_3$  state may also decay to  $\bar{D}D$  without violating conservation laws and ought to have a comparable total width, at least 10 MeV. It would have partial widths to  $J/\psi$  inclusive decay modes comparable to  $\psi(3770)$ .

The masses of charmonium  $D$  states have been estimated. A recent estimate based upon a relativistic formulation gives a  $^3D_2$  state mass of about 3800 MeV and a  $^1D_2$  state mass of about 3790 MeV [15]. Previous estimates give comparable values, [16] also well below the  $DD^*$  threshold of 3875 MeV.

The  $J=2$   $D$  states are expected to be narrow because neither has a decay channel into open charm. The  $^3D_2$  cannot decay into  $\bar{D}D$  or into 2 gluons. Its remaining decay modes are 3 gluons and hadronic and radiative decays to  $\chi$  states and the  $J/\psi$ . The  $^1D_2$  state cannot decay to  $\bar{D}D$  and decays primarily to 2 gluons and to radiative and hadronic modes

including the  $J/\psi$  or another charmonium state. Table 2 gives the decay modes of these states.

Table 2: Decay Modes of Spin 2  $D$  States

Decays of $^3D_2$	Decays of $^1D_2$
$J/\psi\pi^0$ (I-spin forbidden)	$J/\psi\pi^+\pi^-$ (I-spin forbidden)
$J/\psi\eta$	
$J/\psi\pi\pi$	
$\chi_0\gamma$ (0.04 keV [17])	$^1P_1\gamma$ (108 keV [18])
$\chi_1\gamma$ (82 keV)	$J/\psi\gamma$ (1.5 keV)
$\chi_2\gamma$ (31 keV)	$\psi'\gamma$ (0.006 keV)
3 gluons (0.3 MeV, see below)	2 gluons (2 MeV, see below)

Estimates for the partial and total widths of the  $D_2$  states can be obtained from the measured decays of the  $\psi(3770)$  [19] and other charmonium states.

We take the width of the  $^3D_2$  to light hadrons (3 gluons) to be approximately 0.3 MeV, its total width to be 1 MeV and its width to  $J/\psi + X$  to be 70 keV where we sum the contributions of  $J/\psi\pi\pi$  and the E1 transitions  $\chi_1\gamma$  and  $\chi_2\gamma$ . The  $^1D_2$  width is dominated by the 2 gluon decay and is expected to be larger. We take the  $\chi_2$  decay as a guide and estimate 3 MeV for the total width and take 20 keV for the I-spin forbidden width to  $J/\psi\pi^+\pi^-$ . The branching ratios into proton antiproton of the  $\psi'$ , the  $\chi_0, \chi_1, \chi_2$  and  $^1P_1$  are approximately  $10^{-4}$  of the gluonic branching ratio. However the respective ratios for  $J/\psi$  and  $\eta_c$  are about  $10^{-3}$ . One may expect the branching ratios to  $\bar{p}p$  for the  $D$  states to be no greater than  $10^{-4}$  of glue and potentially an order of magnitude less.

We use the above estimates to compute cross sections to  $J/\psi$  inclusive where the  $J/\psi$  decays to an electron pair. For both states we take the rather pessimistic  $\bar{p}p$  branching ratio of  $10^{-5}$ . We find 100 pb for the peak  $^3D_2$  cross section and 10 pb for the peak  $^1D_2$  cross

section.

The acceptance of our detector for a  $J/\psi$  inclusive state is approximately 0.5 as demonstrated in our  $^1P_1$  discovery. The expected cross sections for the  $D_2$  states are similar to the approximately 15 pb (acceptance corrected) that we found for the I spin violating  $J/\psi\pi^0$  decay of the  $^1P_1$ . The expected width for the  $^3D_2$  is comparable to the  $< 1\text{MeV}$  we found for the  $^1P_1$ . The background to  $J/\psi$  inclusive in the  $^1P_1$  and  $\eta'_c$  regions is approximately 6 pb. One would expect it to be roughly the same in the  $D$  region and conclude that the  $J/\psi$  inclusive decay is our best channel.

The strategy of the search for the  $D_2$  state will be the same as for the  $^1P_1$ ; take 1-2  $\text{pb}^{-1}$  of luminosity at intervals separated by 1-2 MeV over the region of interest which is approximately 30 MeV, requiring about 50  $\text{pb}^{-1}$  of integrated luminosity. It is worth noting that the discovery of the  $^1P_1$  has “sharpened” the predictive power of theory. One expects that the anticipated discovery of the  $\eta'_c$  will give theory better capability to accurately predict the  $D_2$  state masses. Since we plan to find the  $\eta'_c$  before starting the search for the  $D$  states, it may be possible to discover the  $D$  states with less integrated luminosity than suggested above. An important piece of physics which is related to the  $D$  state search is the measurement of the excitation cross section for  $D$  and  $\bar{D}$  mesons (open charm). This can be done with a trigger similar to the  $J/\psi$  inclusive trigger, namely an inclusive trigger on relatively low mass electron positron pairs to observe events in which both  $D$  mesons have semileptonic decays into electrons. Data is taken above  $\bar{D}D$  threshold (which includes the data for the  $D$  state search) plus some running below threshold to establish as “charmless” baseline.

## 4. Other measurements done concurrently with the main charmonium program

### Light Quark Spectroscopy

As a result of triggering on the total energy deposited in the central calorimeter, we have acquired in parallel with the Charmonium data a large number of events where light mesons were produced. We first illustrate with some examples the nature of the data, and then discuss possibilities for extending these studies.

### Results from the 1991 run

We show first data from the processes:  $\bar{p} + p \rightarrow 3\pi^0$ ,  $2\pi^0 + \eta$  and  $\pi^0 + 2\eta$ . Fig. 5 a,b show the  $2\pi^0$  mass spectrum for the  $3\pi^0$  and  $2\pi^0 + \eta$  channels respectively for  $\cos\theta_X^*$  in the range 0.2 - 0.6. Apart from the well known  $f_2(1270)$  resonance, the  $3\pi^0$  data shows clearly the  $f_2(1520)$  recently seen in annihilation at rest [20], and further structures at higher mass, which have not been previously seen in antiproton annihilation. We also observe an  $f_2(1520)$  signal in the  $2\pi^0 + \eta$  channel. Measurement of the relative production of  $f_2(1520)$  in these two channels is important, in view of its possible interpretation as a 4-quark or quasi-nuclear bound state [21] [22].

Unlike the  $2\pi^0$  case, the  $2\eta$  spectrum (Fig. 5 c) is almost completely unknown. The features of this are a narrow state at 1500 MeV, possibly the  $f_2(1520)$ , and a striking enhancement at 2.1 GeV which does not correspond to any well-known state, though there exist in the literature [2] several observations of narrow states in this region.

The channels already mentioned, with up to 6 clusters in the Central Calorimeter, are relatively well measured with the present detector. We are also able to study 3-body decays of mesons, (events with 8 photons) and the  $\eta + 2\pi^0$  system is a particularly interesting case. We show in Fig. 5 d the mass plot for the lowest mass  $\eta + 2\pi^0$  combination from the channel:  $\bar{p} + p \rightarrow 3\pi^0 + \eta$ . Here we see the  $\eta'(958)$  in its 3-body decay mode, and a clear signal

identified with the  $f_1(1285)$ .

**Future Program** It is clear from what we have seen that this experiment can study a wide range of light-meson states, not possible anywhere else including LEAR. We now discuss some particularly interesting topics which we wish to pursue.

**Study of the  $f_2(1520)$**  Further investigation of this unique state, seen only in  $\bar{p}p$  annihilation, is clearly very important. A spin-parity analysis of the  $2\pi^0$  system is in progress, using the 1991 data. As well as this, measurement of its branching ratio to eg  $2\eta$ ,  $4\pi^0$  would obviously help in understanding its nature.

**Search for new States decaying to  $\eta+\eta$ ,  $\eta+\eta'$  and  $\omega+\omega$ .** With a larger sample of data on these rarer channels, we will be able to clarify the status of some of the new states which have been reported, eg by the GAMS collaboration, and search for others. The interest here centers on glueballs and hybrid mesons which are predicted in the 2 GeV mass region.

**The  $f_1(1285)$ ,  $f_1(1420)$  and Search for Exotics** The whole question of the nature of the  $a_0(980)$ , possibly a  $K\bar{K}$  state, and its relation with the other states around the  $K\bar{K}^*$  threshold is extremely interesting. The mass-range 1350-1500 MeV is known to contain several states eg  $f_1(1420)$  and  $\eta(1440)$  decaying to  $a_0(980) + \pi$ , whose nature is quite controversial. We have also investigated the channel with  $4\pi^0 + \eta$  in the final state which has been suggested as a possible place to look for exotic mesons in the 2-2.5 GeV mass range

**$\phi$  Physics** Since we see a very clear  $\omega(783)$  signal, in the present data, we should be able to detect the  $\phi(1020)$  in the same way, decaying to  $\eta+\gamma$  (B.R. = 1.28%). The ability to do this could lead to some very interesting physics, eg exotic states [21]. With the present solid-angle coverage, we are as yet unable to extract a significant  $\phi$  signal. The inclusion of a Fitch Cerenkov Counter (see section 6 below) to detect  $\phi \rightarrow K^+K^-$  in pairs would greatly enhance this physics, eg  $\bar{p} + p \rightarrow \phi + \phi + \pi^0$ , and studies of the  $\phi + \phi$ ,  $\phi + \pi^0$  systems.

## Topics with the Upgraded detector

With the acceptance proposed for the  $^1P_1$  discussion in section 2, we will be able both to study an increased range of production angle of the states, and to eliminate background due to unseen products. We illustrate this using the process  $\bar{p} + p \rightarrow \pi^0 + X(1500)$ , where  $X \rightarrow 2\pi^0$ . Fig. 6 shows the acceptance for various ranges of angular coverage, generating decays of the X according to phase-space. The present detector covers the range  $10^\circ - 70^\circ$ . We see that including the forward cone,  $3^\circ - 70^\circ$ , gives very little increase in acceptance (15%), without also covering the backward direction. On the other hand extending our coverage in the range  $70^\circ - 140^\circ$ , as described in section 2, gives a 270% increase in acceptance.

In general, backward produced particles will have low energy, with photon energies up to a few hundred MeV. In the present data, these constitute a background which cannot be eliminated by kinematic fitting, given our resolution, and are particularly serious for rarer channels eg involving  $\eta'$  or  $\omega(783)$ , and for higher multiplicity final states. Thus the proposed enlargement of the detector will make an enormous difference to the quality of the data in most of the channels mentioned above.

**The Drell-Yan process and 4-quark states** It has been suggested that Drell-Yan produced electron-positron pairs in antiproton annihilation might be accompanied by 4-quark mesons [23]. The results of a Monte Carlo simulation using the geometry of our present detector are shown in Fig. 7. Fig. 7a is the expected invariant mass of the  $e^+e^-$  pair and Fig. 7b the recoil mass.

We have analysed a sample of approximately  $440nb^{-1}$  from the 1991  $\psi'$  scan, selecting clean  $e^+e^-$  pairs. The mass distributions are shown in Figs 7c, 7d. The measured cross-section for  $e^+e^-$  masses greater than 1 GeV is found to be approximately 15% of the expected value, 0.8 nb [23], probably due to the fact that the trigger was optimized for higher-mass  $e^+e^-$  pairs.

In future runs we expect to be able to collect several hundred thousand Drell-Yan events,

which will enable us to make an effective search for such 4-quark states. At the same time, we will be able to study cleanly the spectrum of vector mesons in the 1-2 GeV region, by means of their  $e^+e^-$  decay mode.

### **Electromagnetic form factors of the proton**

The electromagnetic form factors of the proton have been measured, for the first time at high  $q^2$  in the time-like region by E760 [24]. The uncertainty on the experimental point at the highest energy was around 35%. With the proposed increase in the total integrated luminosity we expect to improve this measurement to 10%.

## **5. Luminosity upgrade**

### **The upgrade program of the E760 internal target system**

#### **Performance of the present system.**

A diagram of the target system of E760 is shown in Fig. 8. The system consists of the expansion stage, the sink stage, two differential pumping stages on each side and an additional pumping system acting on the accumulator vacuum chamber. A schematic view of the system is shown in Fig. 9. The nozzle geometry has been designed for the following expansion conditions:  $T = 77^\circ \text{ K}$ , (liquid nitrogen) and  $P = 12 \text{ bar}$ ; it has a diameter of  $25 \mu\text{m}$  and a special geometric shape (trumpet nozzle). Out of a flux of  $10 \text{ torr} \times \text{liter/sec}$  of molecular hydrogen ( $\text{H}_2$ ) passing the nozzle throat, the useful fraction of  $\text{H}_2$  in cluster form is about 1%. This corresponds to a target density of  $\sim 0.75 \times 10^{14} \text{ atoms/cm}^3$ . The transverse shape of the beam is shown in Fig. 10.

During the 1991 running the lifetime of the antiproton beam was determined by the target density (that is the amount of gas flowing in the 'jet'), by the amount of gas entering the experiment vacuum chamber but not absorbed by the sink system (diffused gas) and by the residual gas present in the Antiproton Accumulator vacuum chamber.

## **The Target upgrade program.**

For the next run we propose to increase the density of the internal target. The power of the proton cooling system of the Antiproton Accumulator is such that a value of the target density larger than  $10^{14}$  atoms/cm<sup>3</sup> of H<sub>2</sub> can be envisaged. An upgrade of the cooling system of the Accumulator could give us the possibility to use even larger densities.

The increased target density can be obtained with new conditions for the expansion parameters. A lower temperature of the nozzle (with respect to the present 77°K value) will:

- 1) increase the efficiency of the process of clusterization;
- 2) reduce the speed of the H<sub>2</sub> clusters (the speed is proportional to  $\sqrt{T}$ ) hence increase the target density. In fact the target density is inversely proportional to the speed of the clusters.

The new expansion system is being designed as a collaboration of the Genoa group and the Fermilab Research Division. It will use a cryogenerator to cool the nozzle to a temperature in the range 20-25° K. This will require a complete modification of the existing expansion stage. The nozzle will be directly attached to the cold finger of the cryogenerator and the first skimmer will be cooled to liquid nitrogen temperature. Using the same flux (10 torr × liter/sec) and the same geometry for the collimation of the cluster beam, we should obtain a target density increase of 2.5. A preliminary design of the new expansion stage is shown in Fig. 11. To implement this modification in the actual target system we need also to change the mechanics for the pumping in the expansion chamber. This requires the construction of two new vacuum fittings but no major modification of the gas jet proper.

## **Antiproton beam**

The typical beam lifetime, peak luminosity and gas jet intensity achieved during the 1991 fixed target run is summarized in Table 3  $\tau_{on}$  and  $\tau_{off}$  are beam lifetime with gas jet on and off respectively.  $L_0$  and  $d$  are peak luminosity and gas jet density respectively.

Table 3: 1991 Fixed Target Run Summary

Energy	$\tau_{on}(\text{hr})$	$\tau_{off}(\text{hr})$	$L_0(10^{-30}\text{cm}^{-2}\text{sec}^{-1})$	$d(10^{14}\text{Atoms cm}^{-2})$
Stacking		330		
$\psi'$ , $^1P_1$ , $\eta'_c$	89	350	9.1	0.35
$J/\psi$ , $\eta_c$	59	240	3.5	0.35

The goal of the Antiproton source during the collider run is to increase the  $\bar{p}$  stacking rate by a factor of 3 from  $2 \times 10^{10}/\text{hr}$  achieved at the end of 1989 collider run to  $6 \times 10^{10}/\text{hr}$  after the Linac upgrade. We will assume that the  $\bar{p}$  beam intensity for this experiment will be 3 times higher than the 1991 fixed target run in the following. We have calculated the running conditions to produce the maximum integrated luminosity as a function of gas jet density and the results are given in Table 4.

Table 4: Optimal Integrated Luminosity

$d(10^{14}\text{Atoms cm}^{-2})$	Integrated Luminosity
0.35	$\mathcal{L}$
$2 \times 0.35$	$\frac{5}{3}\mathcal{L}$
$3 \times 0.35$	$2\mathcal{L}$

The integrated luminosity is optimized with the assumption that the overhead for deceleration and change over between data taking and  $\bar{p}$  stacking is 16 hours and the beam lifetime as a function of gas jet density is calculated from  $\tau_{on}$  and  $\tau_{off}$  in Table 3. In all cases, the optimal data taking time is  $\approx 1$  beam lifetime. Note that the integrated luminosity does not scale with the gas jet density because the beam lifetime is almost inversely proportional to gas jet density. We see that the goal of improving the integrated luminosity by a factor of 5 can be achieved if both the gas jet density and beam intensity increase by a factor of 3.

The RMS emittance growth due to beam-gas scattering and intrabeam scattering has been calculated and the results are given in Table 5. The beam intensity is taken to be 40 mA. The 95 % emittance is  $2\pi$  mm-mrad ( RMS  $\epsilon = 0.33$  mm-mrad).  $\frac{\sigma_x}{P}$  is  $5.6 \times 10^{-5}$  and  $1.5 \times 10^{-3}$  for  ${}^1P_1$  and  $\eta_c$  respectively. Note that at both energies, even in the case that the gas jet is on, the intrabeam scattering dominates the beam gas scattering.

Table 5: Horizontal Emittance Growth Rate  $\frac{1}{\epsilon} \frac{d\epsilon}{dt}$  ( $\text{sec}^{-1}$ )

Energy	Beam-gas (Gas Jet Off)	Beam-gas (Gas Jet On)	Intrabeam
${}^1P_1$	$1.30 \times 10^{-5}$	$4.43 \times 10^{-5}$	$28.5 \times 10^{-5}$
$\eta_c$	$3.07 \times 10^{-5}$	$10.5 \times 10^{-5}$	$15.4 \times 10^{-5}$

In the scenario that the beam intensity will be a factor of 3 higher (i.e. 120 mA), the beam heating due to intrabeam scattering will also increase by a factor of 3. But the stochastic cooling rate will be reduced by a factor of 3 because the cooling rate is inversely proportional to the beam intensity. To maintain the same emittances as in 1991 with three times more beam, the stochastic cooling system needs to be improved by a factor of 9 (3 for intrabeam scattering increase, 3 for cooling rate decrease).

$S_\omega \xi / n_T$  as a function of  $\xi G$  is plotted<sup>†</sup> in Fig. 12.  $S_\omega$  is the stochastic cooling rate at the center of symmetric beam frequency distribution  $f(\omega)$ ,  $G$  is the system gain and  $\xi = \pi N f(\omega) / n_T$  where  $N$  is the total number of beam particles and  $n_T$  is the total number of Schottky bands in the stochastic cooling frequency bandwidth.  $S_\omega \xi / n_T$  is proportional to the cooling rate times the beam intensity. We would like to increase it by a factor of 9. We typically ran the cooling system at  $\approx 1$ db signal suppression which corresponds to  $S_\omega \xi / n_T = 0.6$ . We see from the figure that it is possible to increase the cooling by a factor of 2. To get a factor of 9 improvement, a 8–16 GHz bandwidth system which corresponds to increase  $n_T$  by a factor of 2 and thus the cooling rate by a factor of 4 is required.

<sup>†</sup>Joseph Bisognano and Christoph Leeman, LBL-14106

The 8-16 GHz bandwidth system will cool the beam to the same emittances as we had during the 1991 run. Without this system, even when optimized, the beam emittances will be considerably larger than in 1991. We estimate the transverse emittance will be  $\approx 4\pi$  mm-mrad and  $\frac{\sigma_x}{p} \approx 4.2 \times 10^{-4}$ . This leads to a transverse size (95% containment) of the beam at the interaction region of  $\pm 0.5$  cm and  $\Gamma_B = 1.5$  MeV/c<sup>2</sup> in the center of mass at  $^1P_1$  which is unacceptably large.

In Table 6 are summarized the values of the parameters which optimize the integrated luminosity for three values of the target density. In the last line are given the integrated luminosities that one can obtain in a 3 month run.

Table 6: Total Luminosity versus Running conditions

Item	1991 jet density	2 $\times$ 1991 jet density	3 $\times$ 1991 jet density
<i>Gas jet density (atoms/cm<sup>-2</sup>)</i>	0.3 10 <sup>14</sup>	0.6 10 <sup>14</sup>	0.9 10 <sup>14</sup>
<i>Cycle time (h)</i>	123.1	101.7	90.8
<i>Data taking time (h)</i>	80.1	58.7	47.8
<i>Stacking time (h)</i>	27.0	27.0	27.0
<i>Overhead (h)</i>	16.0	16.0	16.0
<i>Total no. of cycles</i>	17.5	21.2	23.8
<i>Stacking rate (mA/h)</i>	4.5	4.5	4.5
<i>Beam lifetime (h)</i>	99.4	57.9	40.9
<i>Luminosity/90 days (pb<sup>-1</sup>)</i>	79	128	165

## 6. Detector upgrade

**Charged particle detectors:** To face the higher instantaneous luminosity and have good background rejection we have to make improvements to the charged particle detection

of E760. The general characteristics we need are the following.

- Fast response and short dead time
- Good angular resolution of the order of  $3\text{ mrad}$  in both  $\theta$  and  $\phi$ .
- Redundancy in both  $\theta$  and  $\phi$  measurement, in order to maintain efficient performance if one layer is missing
- $dE/dx$  measurement
- Small thickness (few % of a radiation length)

To fulfill these requirements using as much as possible of the existing E760 detectors, we propose to build a tracking system completely contained inside the Čerenkov counter (see Fig. 13 and 14) consisting of the following elements:

- The existing H1 hodoscope
- A four layer straw tube drift chamber, with stereo view for  $z(\theta)$  and  $\phi$  measurement.
- A 24-fold scintillator hodoscope (H2') to be used in coincidence with H1 as a veto for neutral trigger. Its thickness ( $4\text{ mm}$ ) will also provide a measurement of  $dE/dx$  with the same resolution as the existing H2.
- A silicon strip detector with cylindrical geometry for  $z(\theta)$  and  $dE/dx$  measurement.
- A modified version of the existing RPC with the drift path reduced to  $\sim 1\text{ cm}$  for  $\phi$  measurement.
- The existing MWPC for  $z(\theta)$  measurement and adding wire readout to solve right-left ambiguity in the RPC drift time measurement.
- The existing H2 hodoscope for triggering and  $dE/dx$  measurement.

The overall small radius of the charged detector allows us to track the  $K^\pm$  coming from the decay of  $(c\bar{c}) \rightarrow \phi\phi$  without significant decay losses.

The expected performances of each element are summarized in Table 7

Table 7: Expected Detector Performance

Detector	$r_{min}$ (cm)	$r_{max}$ (cm)	$\sigma_\phi$ (mrad)	$\sigma_\theta / \sin^2 \theta$ (mrad)	$dE/dx$	N.channels
H1	4.3	4.6	-	-	-	8
Straws	5.5	9.2	1.5	12.2		$80 \times 4 = 320$
Silicon	9.5	11.0	-	5.8	25%	$24 \times 192 = 4608$ $24 \times 24 = 578$ (OR A) $24 \times 12 = 288$ (OR D)
H2'	11.5	12.2	-	-	60%	24
RPC	13.0	15.0	2.3	-	-	80
MWPC	15.0	16.0	18	3.1	-	$3 \times 100$ ( $\theta$ ) $320/4 = 80$ ( $\phi$ )
H2	16.2	16.8	-	-	60%	32

In the following we give a short description of the new proposed detectors.

### Straws

The new straw chamber will be composed of 2 modules, each of them containing one tilted (with 10 degrees stereo angle) and one straight layer, both supported by the same structure. Each layer will contain 80 mylar tubes. The tubes range in diameter from 4.4 to 6.1 mm. Each tube will have a drift time measurement, requiring a total of 320 TDC channels with the standard front-end electronics.

The  $\phi$  measurement will be obtained from the radial drift time in the coaxial tubes, while

the  $z$  measurement will use the stereo angle between the different layers.

In order to solve left-right ambiguities and to reduce the inefficiency of the detector due to the cracks between adjacent tubes, the two modules will be staggered by half element. The single layer inefficiency of the tilted layer, due to the increased distance between tubes at the endcaps, is of the order of 5%.

The existing E760 gas system will be used for the new chamber.

### **Silicon barrel**

The silicon barrel will have an internal radius of 9.5 cm, an external radius of 11 cm and a length of 38.4 cm. It will be composed of 24 slabs of silicon strips ( $3\text{ cm} \times 2\text{ mm} \times 280\text{ }\mu\text{m}$ ). The detectors will be supported by 24 multilayer printed circuit boards which will also contain the read-out electronics. In order to avoid inefficiencies due to cracks, the boards will be positioned at two different radii with a small overlap. The overall thickness is expected to be  $\sim 2\%$  of a radiation length.

The total number of strips is 4608, 196 per slab.

The proposed read-out is a chain developed at CERN [25] by which the analog pulses from the strips are read out using a pulse stretching method which allows for serial-parallel multiplexing. The electronic chain is composed of two parts:

- close to the detector: integrating preamplifier, track-and-hold circuit, analog multiplexer, driving amplifier;
- at the counting room: receiving amplifier, ADC and buffer memory.

A complete readout cycle takes  $\simeq 100\mu\text{s}$ .

### **Calorimeter upgrades**

The Calorimeters, particularly the Central Calorimeter which is the crucial element in the

experiment apparatus, worked very well throughout E-760. There were essentially no hardware failures, the energy resolution was adequate and most importantly the segmentation proved adequate for determining event topologies and for obtaining the designed rejection of symmetric  $\pi^0$ 's simulating single photons. The upgrades to the calorimeters are motivated by the same requirement as our desire to increase the instantaneous luminosity. That is we wish to identify and measure states of smaller cross-section, particularly in the  $\gamma\gamma$  decay mode. We concentrate here on decays such as  $\eta'_c \rightarrow \gamma\gamma$ .

Given the excellent rejection of symmetric  $\pi^0$ 's, the major improvement in background rejection available is in the detection of the low energy photon from asymmetric  $\pi^0$  decays. Table 8 shows the signal to background expected at the  $\eta'_c$  for an acceptance with  $|\cos \theta_{cm}| \leq 0.4$  for various values of the energy threshold for detecting a photon.

Table 8: Signal/Background as a Function of Photon Energy Threshold at the  $\eta'_c$

Energy Threshold (MeV)	Signal/ Background
0	8.8
20	2.9
25	2.6
50	1.3
75	0.8
100	0.5

In the case of the  $\eta'_c$  we first have to find the mass of the state. Fig. 15 shows the luminosity needed per point of an energy scan to observe a three sigma effect in the measured cross-section as a function of the signal to background ratio. It should be noted that the vertical axis scales as  $n^2$  where  $n$  is the number of sigma desired for the observed effect. Below a signal-to-background ratio of  $\approx 3$ , the luminosity required increases rapidly. Referring to table 8 this leads to our goal of a 20 MeV threshold. Analysis of our present data shows

an effective threshold of about 30 MeV. There is enough light generated in the lead-glass to allow us to detect energy deposits down to 10 MeV and we need to increase the dynamic range of our signals compared to the noise level in the system. For much of the array, this can be achieved with our present ADC's; we are studying the issue in detail for the forward part of the apparatus but do not anticipate any major difficulties here either.

A much more serious concern arises from the increase in interaction rate which could lead to event pile-up. Since the experiment depends on identifying exclusive channels, one approach might be simply to reject from consideration any events which do not have the exact characteristics of the specified mode. For example, events which do not have exactly two energy deposits would be excluded from searches for  $\eta'_c \rightarrow \gamma\gamma$  unless we could identify the extra energy deposit as being out of time. We have calculated the effect of such a cut using our present data by taking a very clean and large signal, the  $\chi_2 \rightarrow \psi + \gamma, \psi \rightarrow e^+e^-$ . Table 9 shows the efficiency for the  $\chi_2$  signal as a function of the energy threshold for identifying deposits as out-of-time at the E-760 luminosity and at the P-835 luminosity.

Table 9: Efficiency versus the threshold for identifying energy as Out-of-Time

Threshold (MeV)	Efficiency at $10^{31}/cm^2$	Efficiency at $5 \times 10^{31}/cm^2$
20	1.0	1.0
25	0.94	0.71
35	0.89	0.55
50	0.83	0.40
100	0.76	0.25
200	0.71	0.18

In the E-760 setup, we have latches on sums of 8 blocks with effective threshold of 200 MeV. It is clear that at the luminosity we need it is essential to identify the timing of energy

deposits as small as 20 MeV. There are several ways to achieve this under consideration - including ADC's with an early gate on each channel and putting a discriminator on each channel with its output going to either a TDC or a latch with a narrow ( $< 20ns$ ) gate at the event time. In all cases, this implies a fairly significant increase in the amount of electronics per channel. The number of channels (1500) involved, however, is relatively modest. We will make a choice based on effectiveness, including the amount of data to be read out, and feasibility of implementation considering time and cost.

### Trigger System

The trigger system is made of two levels:

1) level 1 is a fast logic trigger ( $\sim 100$  nsec) to select:

a) events with electron pairs and/or  $\gamma$  pairs with large invariant mass

( $\chi_{0,1,2}, {}^1P_1, \psi', {}^1D_2, {}^3D_2 \rightarrow J/\psi(\rightarrow e^+e^-) + X, J/\psi \rightarrow e^+e^-, \chi_{0,2}, \eta_c, \eta'_c \rightarrow \gamma\gamma, {}^1P_1 \rightarrow \eta_c(\rightarrow \gamma\gamma)\gamma$ );

b) neutral final states with a large fraction of the total energy deposited in the calorimeters ( $\eta_c, \eta'_c \rightarrow \eta\eta\eta, \eta\pi^0\pi^0, {}^1P_1 \rightarrow \eta_c(\rightarrow \eta\eta\eta, \eta\pi^0\pi^0)\gamma$ ) and annihilation processes into any combinations of  $\pi^0, \eta, \eta', \omega$

c) four charged tracks with two close pairs ( $\eta_c \rightarrow \phi(\rightarrow K^+K^-)\phi(\rightarrow K^+K^-), {}^1P_1 \rightarrow \eta_c(\rightarrow \phi\phi \rightarrow 4K^\pm)\gamma$ );

d) two body reaction final states ( $\bar{p}p \rightarrow \bar{p}p, \pi^+\pi^-, K^+K^-$ ) with prescaling.

The total rate at the first trigger level output has to be contained below  $\bar{1}0$  kHz, which is the limit of the manageable rate of the Level 2 trigger.

2) level 2 trigger is based on a set of  $\geq 6$  VME processors, which is described in the DAQ upgrade subsection.

For simplicity, the description of the logic will be divided into two subsystems: a) the

charged trigger, based on the scintillator hodoscopes and the Čerenkov counter; b) the calorimeter trigger, using summed outputs of the calorimeter signals.

### Charged Trigger Description

Based on the experience gained from E760, the charged trigger will be mainly used, together with the calorimeter trigger, to obtain fast and effective selection of events with an electron pair of large invariant mass. This event category includes several interesting decay channels from  $J/\psi, \psi', \chi_{0,1,2}, {}^1P_1, {}^{1,3}D_2$ . The hadronic decay chain  $\eta_c \rightarrow \phi\phi \rightarrow 2K^+2K^-$  will be selected by a different logic using the charged trigger elements. The hodoscopes signals will also be used as a veto in the neutral trigger logic.

We propose some changes with respect to E760, with the aim of being better equipped to cope with higher luminosity and of improving our background rejection. As in E760, plastic scintillator hodoscopes H1(8 counters) and H2 (32 counters), coaxial to the beam line, will signal the passage of charged tracks, the gas threshold Čerenkov counter will be used to tag electrons, and the forward counters will veto tracks at small polar angle. No modifications are envisaged for these detectors, except possibly a new light collection system for H2. To allow room for the new backward detectors, we are investigating the possibility of reading this hodoscope out at the downstream end of the apparatus.

From what was learnt from E760, maximum benefit for the experiment comes from a careful mix of the charged and calorimeter triggers. Electron identification, a powerful feature of the charged trigger, combines very effectively with the energy measurement capability and uniformity of response of the calorimeter, providing high selectivity and good efficiency over the large acceptance of the experiment.

(a) For the  $e^+e^-$  trigger, we will keep the same logic that worked well in E760 as the OR of 3 subtriggers:

$$1) T_{e^+e^-}^{(1)} = (H1 \times H2^{sect} \times C)_i \times (H1 \times H2^{sect} \times C)_j \times mult(H2) \times copl(H2) \times PBG1$$

where:  $H2^{sect}$  is the OR of a number of  $H2$  elements corresponding in azimuthal angle to a given  $H1$  element,  $mult(H2)$  is a requirement on the  $H2$  multiplicity;  $copl(H2)$  is a requirement on two tracks coplanarity as found by  $H2$ ,  $PBG1$  is a calorimeter trigger, requiring two clusters above threshold with large ( $> 90^\circ$ ) azimuthal opening.

$$2) T_{e^+e^-}^{(2)} = (H1 \times H2^{sect} \times C)_i \times (H1 \times H2^{sect})_j \times mult(H2) \times copl(H2) \times PBG1$$

where everything is the same as in  $T_{e^+e^-}^{(1)}$  except for a tighter  $H2$  multiplicity requirement. This will be implemented to monitor the Cherenkov efficiency.

3)  $T_{e^+e^-}^{(3)}$  as  $T_{e^+e^-}^{(1)}$  without requirements on  $PBG1$  and a tighter  $H2$  multiplicity constraint. This last trigger will be implemented to monitor the calorimeter efficiency.

(b) In order to trigger on  $\phi\phi$  final states, a special logic will be implemented, based on a scheme already tested for a short period in E760. We plan to have the following charged trigger:

$$T_{\phi\phi} = (H1 \times H2^{sect})_i \times (H1 \times H2^{sect})_j \times mult(H2) \times copl(H2) \times \overline{veto} \times clust(H2) \times mult(H1) \times \overline{CCAL(ring1 \rightarrow ring5)}$$

where:  $mult(H2)=3$  or  $4$  is a requirement on the  $H2$  multiplicity,  $clust(H2) = 2$  or  $(3$  and  $1$  gap) is a requirement on the  $H2$  pattern, that there be either two clusters of  $H2$  counters or 3 clusters with a gap of 1 counter between two of the clusters,  $\overline{veto}$  includes the new backward detector and the forward veto hodoscopes,  $mult(H1) < 4$  is a requirement on the  $H1$  multiplicity,  $\overline{CCAL(ring1 \rightarrow ring5)}$  is a calorimeter veto to exclude from the acceptance regions where the background is expected to be high and the signal small.

We collect in Table 10 the projected trigger rates for selected reactions.

For  $e^+e^-X$ , the rates are projections from E760 measured rates to P835 luminosities.

For  $\phi\phi$  and  $\phi\phi\gamma$ , the rates are obtained from E760 test runs and simulations of a number of background reactions accounting for more than 50 % of the measured rate. Altogether, the quoted rates are estimated to be realistic within a factor 2.

Table 10: First Level Trigger Rates

Reaction	$E_{cm}$ (GeV)	Inst. Lumin. $10^{31} \text{ cm}^{-2} \text{ sec}^{-1}$	Fast trigger rate (Hz)	Remarks
$e^+e^- X$	2.980	2.0	25	From E760 data
"	3.097	2.0	30	"
"	3.526	5.0	125	"
$\phi\phi$	2.980	2.0	820	From E760 data and Montecarlo
$\phi\phi\gamma$	3.526	5.0	1300	From E760 data and Montecarlo

### Neutral Trigger

The Neutral Trigger hardware in E-760 consisted of two major items: a total energy sum of all 1280 counters in the Central calorimeter and a set of 40 energy 'sums' (8 in  $\phi$  and 5 in  $\theta$ ) of 40 counters. The energy sum was required to exceed a given threshold (typically 90% of the available energy) and was used for inclusive neutral events. The cluster sums were used for two body decays by setting a  $\theta$  dependent threshold on the sums and requiring two sums to fire with  $\Delta\phi > 90^\circ$ .

This scheme produced a trigger rate of  $\approx 1$  kHz into the Level 2 microprocessors. While we plan to improve the rate capability of the electronics where necessary, we do not anticipate a major improvement in rejection. As a consequence, the event read-out time must be reduced and the level 2 processing power increased to cope with the increased data to avoid excessive dead-time. This is described in the next section.

An aspect of the neutral trigger which will require hardware improvements is the charged particle veto and a new detector, the H2' scintillator hodoscope, has been designed to this end. In E760, the veto action was performed by H1, which was built explicitly to match

the polar acceptance of the central calorimeter. However, we found a serious problem with this since the total H1 rate is affected by the large  $\delta$ -ray production in the source, resulting in a sizeable random veto. The new H2' will have higher segmentation and the same polar acceptance as H1, covering  $\theta$  down to  $9^\circ$ , the veto action being performed by the coincidence  $H1 \times H2'$ . (On the other hand, we will keep the existing H2, rather than H2', to define the polar acceptance of the charged trigger, in order to avoid the large increase in trigger rate coming from small angles and to match the Čerenkov acceptance.)

We are also considering the usefulness of inserting another anticounter array just around the beam pipe, in order to veto against beam-gas interactions downstream the target. This would consist of 8 scintillator bars placed along the beam pipe, with the same readout structure as H2 and H2'.

### **Data Acquisition upgrade**

Experiment E760 collected data at a maximum trigger rate of 1 kHz with a 15% deadtime. A new high rate data acquisition system is necessary for the next run due to the anticipated 5-fold increase in instantaneous luminosity. The major upgrades that will be done within the next two years are described below.

In E760 the CAMAC crates were read-out through their CAMAC back-plane to Fermilab RBUF buffers via the Fermilab Smart Crate Controllers. Most of these crates contain the LeCroy Fera ADCs which provide a fast readout via their ECL port. This readout can reach a speed of 100 ns/word which is 10 times faster than the corresponding readout via the CAMAC dataway. To speed up the readout, P835 plans to read-out all its data via the ECL port and is selecting its electronics accordingly.

The Fermilab RBUF buffers will be replaced by 8 Q+ modules. These new buffers are integrated I/O controller and dual ported VME memory modules being designed and implemented by the Fermilab Computing Division. These modules are single width, 6-U high, VME-resident units, capable of sustaining an overall throughput rate of 20 Mbytes/sec.

The maximum expected data rate for P835 is about 5 Mbytes/sec. Buffer management is handled by a local processor. The Q+ modules comply fully with the VME slave interface specifications, providing for random or block transfer operations.

23 ACP modules served as the Level 2 processors for E-760. These will be replaced by a system of at least 6 Motorola MVME167 single board computers, running VxWorks as operating system. The MVME167 is based on the MC68040 microprocessor which is about 25 times faster than the ACP one. It has SCSI and Ethernet ports and provides for block transfers over the VME backplane at a rate of 20 Mbytes/sec. The total CPU power of the system (100 MIPS) is more than 6 times the one available in E760. A test is under way to estimate the exact number of the MVME167 modules. Space is available in the VME crate for up to 5 additional modules, which would almost double the CPU power of the system, in case more CPU power is needed. The experiment plans to rely on the Fermilab computing division to provide general system and environment support for code development and the use of VxWorks.

The system will be configured in a way similar to the ACPs. One MVME167 will be the "boss" and the rest the "slaves". The "boss" will poll the "slaves" and assign one at a time as "master" of the VME. The "master" will read the data from the buffers while the other "slaves" are analyzing and filtering events. When a "slave" finishes filtering the events in its input buffer, it informs the "boss" which reads the "slave's" output buffer. The "slave" will then wait to be assigned as "master". The "boss" logs the data to 8mm tapes, in the drives connected to its SCSI port. The "slave" also sends its data over its Ethernet port to a pool in a Unix workstation. Monitor programs running in that workstation read the data from the pool and fill histograms. The number of tape drives depends on the filtering factor achieved by the processors and on the maximum logging rate of the drive. The data rates logged by E760 are given in Table 11. Given rewind and reload time, two sets of three of the new Exabyte EXB-8500 tape drives are estimated to be sufficient.

The "run control" program resides in the host Unix workstation. It initializes the proces-

Table 11: Trigger Rates from E-760

	$\eta_c$ (2.98 GeV)		$^1P_1$ (3.53 GeV)	
	Trigger rate	Rate to tape	Trigger rate	Rate to tape
Neutral (Hz)	1034	219	716	189
Charged (Hz)	7	6	22	19
Instant. lumin. ( $cm^{-2}s^{-1}$ )	$5 \times 10^{30}$		$7.9 \times 10^{30}$	
Live time	0.83		0.85	

sors, downloads the filtering code over their Ethernet ports and starts or stops it. During the run, the program displays the status of the Data Acquisition and any errors the processors may detect. The E760 filtering code will be updated and converted to C to be compatible with the VxWorks operating system. The initialization of the CAMAC crates will still be done from a Vaxstation 3100 through two Jorway parallel branches and A-2 crate controllers. In all this scheme, the experiment is relying on being able to use the software being developed by the Online Support group in the Computing Divisions under the DART project.

The data acquisition architecture for P835 is shown in Fig. 16.

## 7. Other measurements

In this section we discuss measurements which require some modification of the experimental setup. Such modifications will present a serious disruption in data taking and will not be undertaken before the higher priority items are accomplished.

### $\phi\phi$ final states

Events with two  $\phi$  in the final state are interesting from a variety of points of view:

- 1) study of the  $\eta_c$  through the decay  $\eta_c \rightarrow \phi\phi$  is complementary to that done with  $\eta_c \rightarrow \gamma\gamma$

providing additional information on the resonance width ( $\sim 40\%$  error with  $20 \text{ pb}^{-1}$ ). It also yields a precise measurement ( $\sim 25\%$ ) of the product of the branching ratios to  $\bar{p}p$  and to  $\phi\phi$ . The detected peak cross section, of the order of  $130 \text{ pb}$ , compares favourably with the  $\sim 30 \text{ pb}$  of the two photon channel; however the signal/background ratio is estimated to be 2-3 times smaller, as the resonance sits over a continuum of annihilations into  $\phi\phi$ . [26]

2) As a by-product of the  $\eta_c$  studies, several thousand non resonant annihilations into  $2\phi$  will be collected allowing a high statistic study of this OZI suppressed reaction.

3) The search for the decay  $^1P_1 \rightarrow \eta_c\gamma$  may profit from detection of the  $\eta_c$  from its  $2\phi$  decay. The signal is estimated to be  $9 \text{ pb}$ , and the background is of instrumental origin and is estimated from Monte Carlo to be about two times the signal.

4) the study of the  $\phi\phi\pi^0$  channel will allow a search for exotic  $\phi\phi$  states.

With the P-835 apparatus as discussed, the  $\phi$  can only be detected through its charged decay to  $K^+K^-$ ; detection of a double  $\phi$  therefore implies detecting 4 charged  $K$ 's in the final state, possibly with an extra photon or  $\pi^0$ . The detection of these states is a rather formidable task from the point of view of the hadronic suppression both at the trigger level and in the offline analysis. This is based on topological filters and on a 2C kinematical fit, with the  $4K$  momenta unknown and good angular resolution ( $\sim 3 \text{ mrad}$ ) is therefore required. Due to the low Q value of the  $\phi$  decay and to the narrow width of the  $\phi$ , the real events have very special configurations and the fit is highly selective against background. Nevertheless it has been proved by R704, with a similar apparatus and technique, that at  $E_{cm} \simeq 3 \text{ GeV}$  a background of the same order of the signal survives all cuts and must be statistically subtracted [26].

At the  $\eta_c$  formation energy, we have the option of using a special Čerenkov Fitch-type spherical glass counter [27] (based on total internal reflection) acting as a charged  $\pi$  veto (see Fig. 17). This instrument in the version that is being built would replace the gas threshold Cherenkov counter. The Fitch counter can distinguish particles with  $\beta < 0.92$  from particles

with  $\beta > 0.94$  and is capable of reducing the first level trigger rate by a factor 4. It may also prove very valuable to reject the background surviving all the filters of the offline analysis and thus to improve substantially the signal to noise ratio.

The rates quoted in section 6 do not account for the Fitch counter veto reduction.

### Charmonium-Nucleon cross sections

Meson-nucleon cross sections constitute some of the most basic experimental information about hadronic interactions. However, the existing experimental knowledge stops at pions and kaons; essentially nothing reliable is known about nucleon collisions with mesons containing charm or beauty quarks. Theoretical understanding of meson-nucleon interactions is even more meager, being limited to the rather ad-hoc potential models. The interaction between nucleons and heavy mesons which do not contain up or down quarks must be mediated by pure gluon exchange, and experimental studies of these collisions can be expected to lead to new insight into the fundamental nature of the interaction. Measurements of charmonium-nucleon cross sections would provide just such data.

In addition to the intrinsic importance common to all charmonium-nucleon cross sections, the  $J/\psi$ -nucleon cross sections have recently acquired an importance all their own. This arises from the identification of the suppression of  $J/\psi$  production as the unique signal for quark-gluon plasma formation in heavy ion collisions. It has been proposed [28] that in the presence of a quark-gluon plasma color screening would prevent the binding of a produced  $c\bar{c}$  pair into a  $J/\psi$  (or  $\psi'$ ), leading to the suppression of  $J/\psi$  production. A suppression of  $J/\psi$  production has indeed been observed in oxygen and sulphur collisions with uranium in the CERN experiment NA-38,[29] and has been interpreted as evidence for the formation of a quark-gluon plasma, or at least an approach to it [30]. The observed suppression can be explained in more conventional terms of nuclear attenuation if  $J/\psi$ -nucleon total cross sections are as large as  $\approx 10mb$ , instead of being  $\approx 2mb$ , as is usually assumed. The small values of  $J/\psi$ -nucleon cross sections come from a Glauber type of analysis of photoproduction of  $J/\psi$  on nuclear targets at 50-200 GeV. However, as Brodsky and Mueller [31] have pointed

out, these values "have little to do with  $J/\psi$  scattering on a nucleon". The reason is 'color transparency'. The  $c\bar{c}$  pair produced at these energies exits the nucleus long before it has time to grow to the transverse dimension of a  $J/\psi$  [ $\tau_{formation} = 1 fm \times p_{\gamma}(GeV)$ ]. The 'small'  $c\bar{c}$  pair has very small color dipole moment and therefore a very small interaction cross section with nucleons. As Brodsky and Mueller have pointed out, the best way to measure the true  $J/\psi$ -nucleon cross section is to produce the  $c\bar{c}$  pair with such small momentum that the  $J/\psi$  is formed well within the nucleus, and the color transparency effect is kept at a minimum level. Resonant production of  $J/\psi$  with  $\bar{p}$  incident on a nucleus is therefore the ideal method.

The  $J/\psi$ -nucleon cross section measurement can be made easily by E760. Except for the broadening of the  $J/\psi$  due to the Fermi motion of the protons bound in a nucleus, the kinematics of the reaction is identical to that of  $J/\psi$  production on a free proton. The same trigger -  $J/\psi \rightarrow e^+e^-$  can be used. Only the hydrogen-gas jet target needs to be replaced by a heavy-gas jet target. Such targets of gases as heavy as krypton are in routine operation in several laboratories, e.g., in the ADONE ring at Frascati. We have studied the feasibility of such targets at E760 and have concluded that targets of gases as heavy as neon can indeed be used with the stochastically cooled antiprotons in the FNAL antiproton accumulator. If the proton density in the heavy-gas jet [ $Z\rho_{atomic}$ ] is kept the same as that in the hydrogen jet, the beam lifetime is expected to be the same as that for the hydrogen jet. In changing from hydrogen to a heavy-gas only the temperature of the gas jet needs to be changed. As mentioned elsewhere in the proposal, the existing jet source is being modified to accommodate a cryogenic refrigerator to cool the jet nozzle to the desired temperature. This will enable us to produce heavy-gas jet targets very conveniently, and to change gases without interfering with the circulating beam.

Fermi broadening of the  $J/\psi$  resonance in a nucleus is estimated to reduce the peak cross section over that for protons by a factor of  $\approx 10^3$ . With an instantaneous luminosity of  $ZL = 5 \times 10^{31} cm^{-2} sec^{-1}$  expected in 1994, this gives  $\approx 1000 J/\psi$  detected /day at the  $J/\psi$  peak. This means that a five point scan of the Fermi broadened peak can be done in a typical

beam lifetime of about 72 hours. Two or three different nuclear targets can be studied in about a week. Measurements with different nuclear targets are useful in confirming that our measurements are indeed uncontaminated by color transparency effects.

It is worth noting that it is also of interest to determine the  $\psi'$ -nucleon cross section at least for one nucleus to see how different it is from the  $J/\psi$  - nucleon cross section. The  $\psi'$ -nucleon cross section is expected to be up to four times larger because of the almost factor two larger radius of  $\psi'$ . However, despite this increase, these measurements are expected to be slower by nearly a factor 20 because of the much lower cross section for the reaction on the free proton.

## Appendix

In Table 12 a comparison is shown between the estimates given in the previous version of the P835 proposal[1] for cross sections, efficiencies and the luminosities required for the planned experiments and the actual measurements subsequently made in the 1991 part of the fixed-target run of E760. The percent errors refer to the measurements of branching fractions for the corresponding channels. The '??' mean that no estimate was given.

Table 12: Comparison of predicted and measured cross-sections and efficiencies

	Decay channel	$\sigma_R$ (pb)	$\sigma_{back.}$ (pb)	<i>eff.</i>	$\mathcal{L} dt$ ( $pb^{-1}$ )	Quality of measurement
Ref [1]	$^1P_1 \rightarrow J/\psi + X$	55	15	0.4	7	$4\sigma$
E-760 meas.	$^1P_1 \rightarrow J/\psi + \pi^0$	18	6	0.32	16	30%
Ref [1]	$^1P_1 \rightarrow (\gamma\gamma)\eta_c + \gamma$	32	15	0.25	15	$4\sigma$
E-760 meas.		$\leq 10(90\%C.L)$	25	0.12	16	<i>not seen</i>
Ref [1]	$\eta'_c \rightarrow \gamma\gamma$	180	15	0.25	5	??
E-760 meas.		-	38	0.28	6	<i>not seen</i>
Ref [1]	$\chi_2 \rightarrow \gamma\gamma$	108	15	0.25	1.5	15%
E-760 meas.		42	42	0.28	2.5	25%
Ref [1]	$\eta_c \rightarrow \gamma\gamma$	560	??	0.2	2.5	??
E-760 meas.		360	240	0.13	3.6	30%

## References

- [1] Proposal to extend E760 activities in the next fixed target run (E760 Collaboration) Fermilab Proposal P835.
- [2] Particle Data Group, "Review of Particle Properties", Phys. Lett. B239,1 (1990).
- [3] W.Kwong et al., Phys. Rev. D37,3210 (1988).
- [4] J.Pantaleone, S-H Tye, Phys. Rev. D37,3337 (1988);  
S.N.Gupta et al.,Phys. Rev. D39, 974 (1989);  
V.V.Dixit et al., Phys. Rev. D42, 166 (1990);  
A.M.Badalyan and V.P. Yurov, Phys.Rev. D42, 3138 (1990);  
L.P.Fulcher, Phys. Rev. D44, 2079 (1991);  
J.Stubbe and A.Martin, Phys. Lett. 271B, 208 (1991);  
D.B.Lichtenberg and R.Potting,Phys.Rev.D (to be published)
- [5] Y-P.Kuang, S.F.Tuan, and T-M.Yan, Phys.Rev. D37, 1210 (1988) M.B. Voloshin, Sov.J.Nucl.Phys. 43,1011(1986)
- [6] T.A. Armstrong et al. Observation of the  $^1P_1$  state of Charmonium, Fermilab-Pub-92/186-E 1992, submitted to Phys.Rev.Lett.
- [7] E.D.Bloom and C.W.Peck, Ann.Rev.Nucl.Sci. 33,143 (1983) and references therein
- [8] T.A. Armstrong et al. Measurement of the  $\gamma\gamma$  Partial Width of the  $\chi_2$  Charmonium Resonance In preparation,to be submitted to Phys.Rev.Lett.
- [9] S.J.Brodsky, G.P.Lepage, Phys. Rev. D24,2848 (1981).
- [10] E.S.Ackleh and T.Barnes Phys.Rev. D45, 232 (1992) and references therein
- [11] G.Bodwin,E.Braaten and G.P.Lepage, ANL-HEP-PR-92-30, NUHEP-TH-92-4, April 1992

- [12] T.A.Armstrong et al., Nucl.Phys. B373, 35 (1992).
- [13] M.Oreglia et al.; Phys. Rev. D25, 2259, (1982);
- [14] K.J.Sebastian, H.Grotch, F.L.Ridener,Jr.; Phys. Rev. D45, 3163, (1992);
- [15] E. Altshuler and D. Silverman UC Irvine Technical Report 92-35 (submitted to Physics Letters).
- [16] W. Kwong et al., Phys. Rev. D37, 3210, 1988.
- [17] F. Daghighian and D. Silverman, Phys. Rev. D36, 3392, 1987.
- [18] Y-P Kuang et al., Phys. Rev. D37, 1210, 1988.
- [19] Y. Zhu PhD thesis CALT-68-1513 1989.
- [20] E.Aker et al, Phys.Lett. B260, 249 (1991)
- [21] C.B. Dover, Summary talk, SuperLEAR workshop, Zurich, Switzerland, 9-12 Oct 1991.
- [22] C.B. Dover et al, Phys.Rev. C43, 379 (1991)
- [23] M. Strickman and G. Ladinsky, Penn State U., private communication.
- [24] T.A.Armstrong et al., Measurement of the proton electromagnetic form factors in the time-like region at 8.9 to 13  $GeV^2$  ,subm. to PRL(1992).
- [25] R. Albergati et al. NIM A 248(1986)337
- [26] C. Baglin et al., Phys. Lett. B231, (1989), 557.
- [27] C. Biino et al., Nucl. Instr. and Methods A295, (1990), 102.
- [28] T. Matsui and H. Satz, Phys. Lett. B178 (1978), 416.
- [29] C. Baglin et. al. (NA38), Phys. Lett. B220 (1989) 471; B251 (1990) 465, 472; Phys. Lett. B255 (1991) 459.

- [30] H. Satz, Proc. International Lepton Photon Symposium, Geneva 1991, edited by S. Hegarty et. al. (World Scientific, Singapore 1992) pp. 273-300.
- [31] S.J. Brodsky and A.H. Mueller, Phys. Lett. B206 (1988) 685.

## List of Figures

- Fig. 1 The measured  $\gamma\gamma$  Event Rate in the region of the  $\eta_c$
- Fig. 2 The measured  $J/\psi + \pi^0$  Event Rate in the region of the  $^1P_1$
- Fig. 3 A schematic of the Backward Detector
- Fig. 4 The measured  $\gamma\gamma$  Event Rate in the region of the  $\eta'_c$
- Fig. 5(a) Invariant mass( $2\pi^0$ ) from the reaction:  $\bar{p} + p \rightarrow 3\pi^0$  for  $\cos\theta_X^*$  in the range 0.2-0.6
- (b) Invariant mass( $2\pi^0$ ) from the reaction:  $\bar{p} + p \rightarrow 2\pi^0 + \eta$  for the same range of production angle
- (c) Invariant mass( $2\eta$ ) from the reaction:  $\bar{p} + p \rightarrow \pi^0 + 2\eta$
- (d) Invariant mass( $2\pi^0 + \eta$ ) from the reaction:  $\bar{p} + p \rightarrow 3\pi^0 + \eta$
- Fig. 6 Acceptance of the detector as a function of  $\cos\theta_X^*$ , for a meson of mass  $1.5 \text{ GeV}/c^2$  decaying to  $2\pi^0$ s in the reaction:  $\bar{p} + p \rightarrow 3\pi^0$
- Fig. 7(a) Invariant mass( $e^+e^-$ ) from a Monte Carlo simulation of the Drell-Yan production of a 4-quark state
- (b) Recoil mass produced in the above simulation
- (c) Invariant mass spectrum from the  $\psi'$  data
- (d) Recoil mass spectrum from the  $\psi'$  data
- Fig. 8 The E-760 Gas-Jet Target General Schematic
- Fig. 9 The E-760 Gas-Jet Target Nozzle Schematic
- Fig. 10 The E-760 Gas-Jet Geometry

- Fig. 11 The P-835 Gas-jet Expansion stage Schematic
- Fig. 12 Antiproton Cooling Rate Parameter Plot
- Fig. 13 A 90° azimuthal section of the P-835 tracking system
- Fig. 14 A longitudinal view of the P-835 tracking system
- Fig. 15 The luminosity per point needed in an energy scan to see a  $3\sigma$  effect as a function of Signal/Background
- Fig. 16 The P-835 Data Acquisition Scheme
- Fig. 17 Schematic of the Fitch Counter

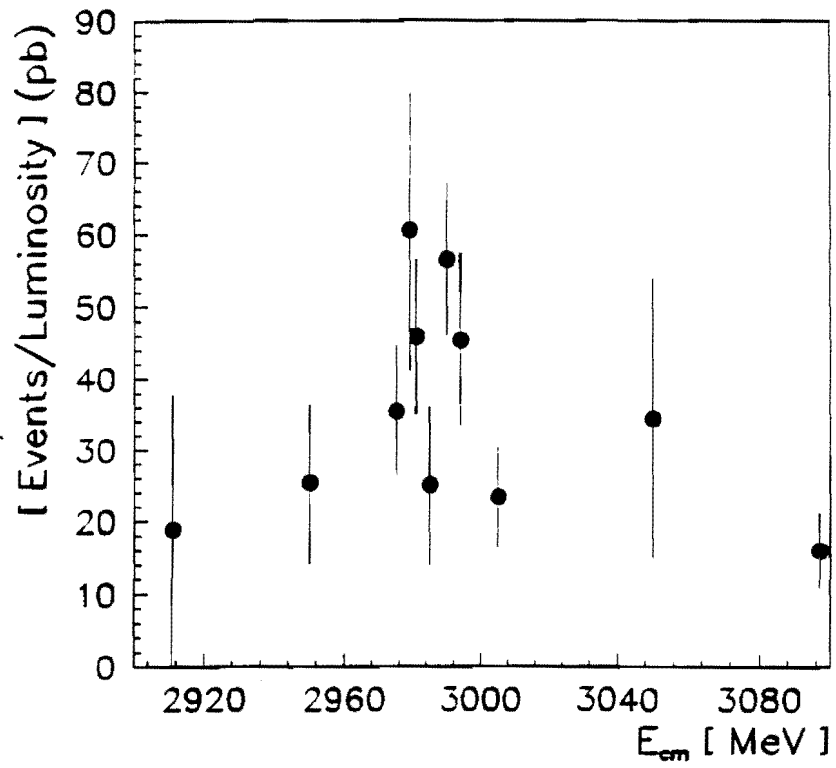


Fig. 1 The measured  $\gamma\gamma$  Event Rate in the region of the  $\eta_c$

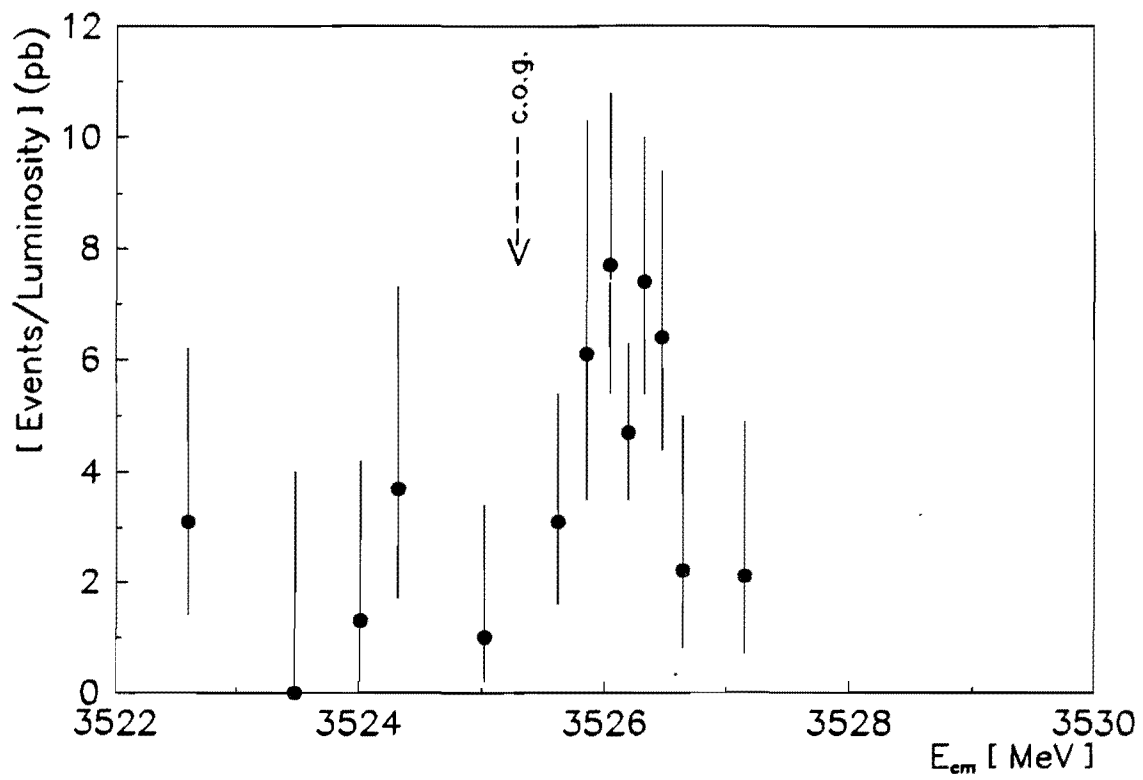
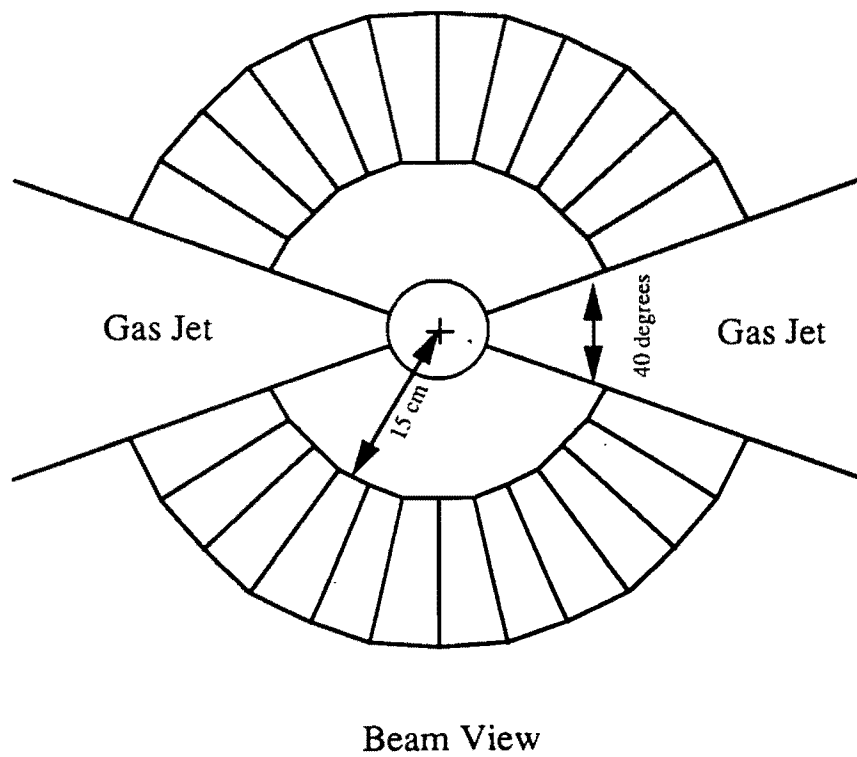
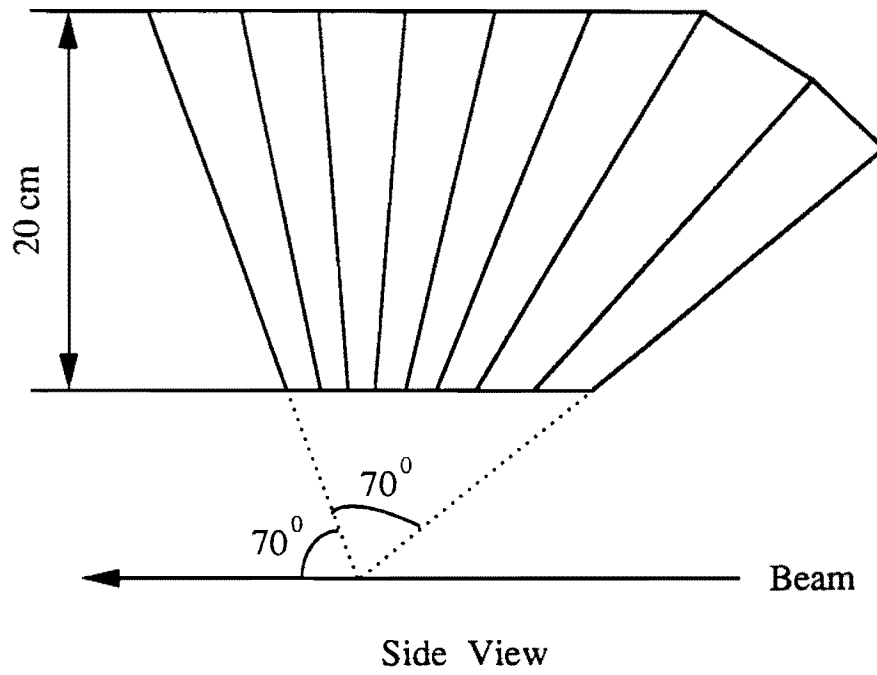


Fig. 2 The measured  $J/\psi\pi^0$  Event Rate in the region of the  $^1P_1$



### Schematic of Backward Photon Detector

Fig. 3 Schematic of the Backward Detector

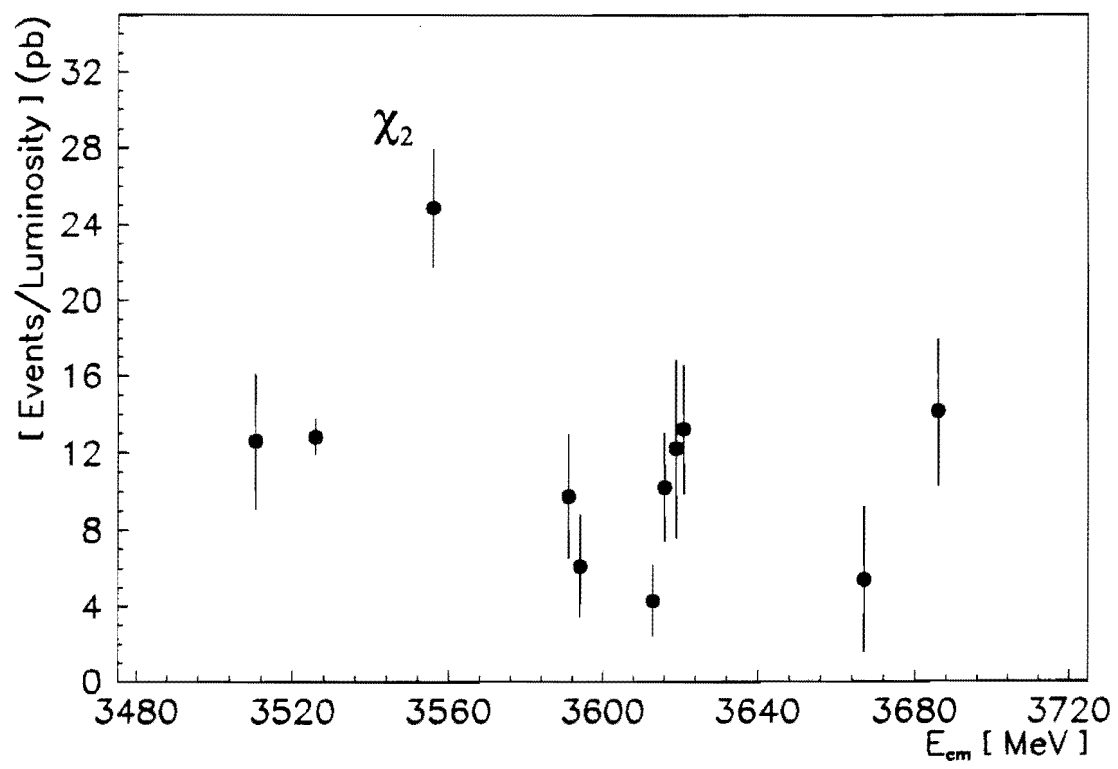


Fig. 4 The measured  $\gamma\gamma$  Event Rate in the region of the  $\eta_c'$

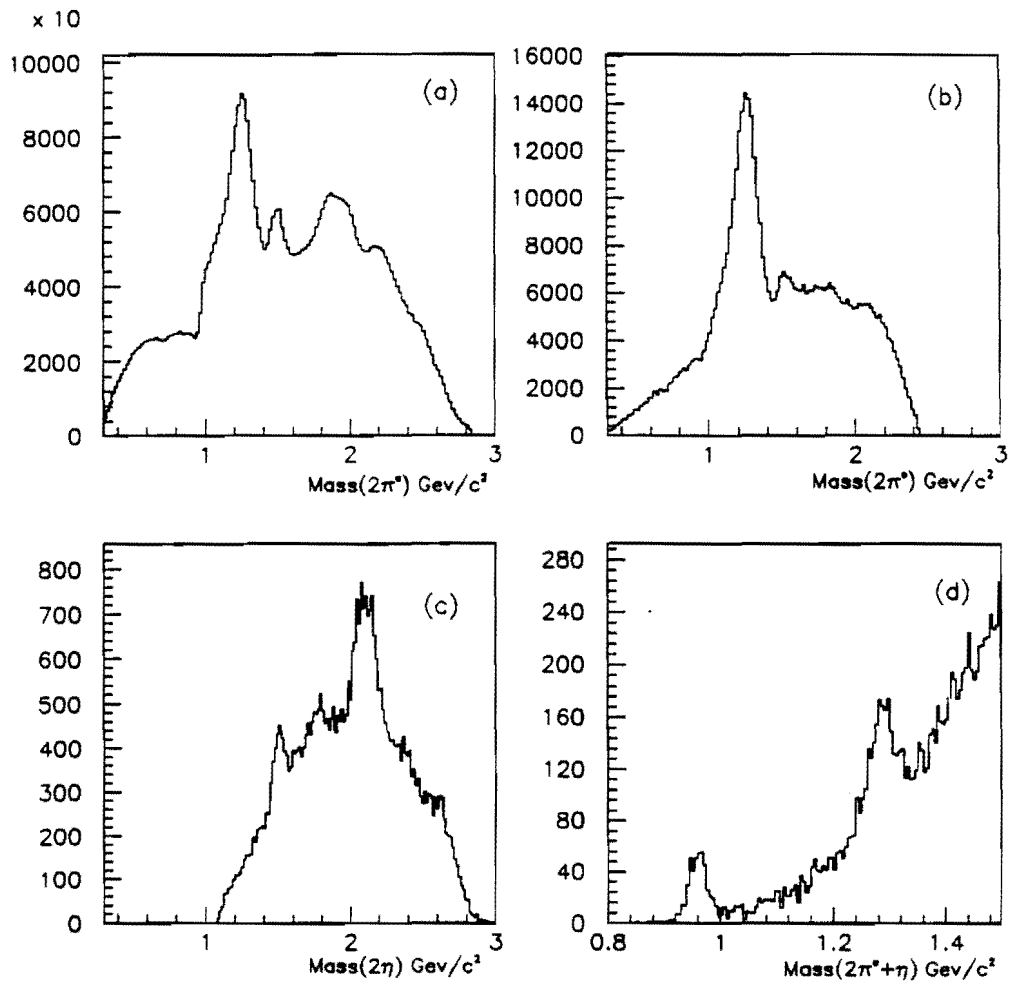


Fig. 5  $\pi^0\pi^0$ ,  $\eta\eta$  and  $\pi^0\pi^0\eta$  mass distributions

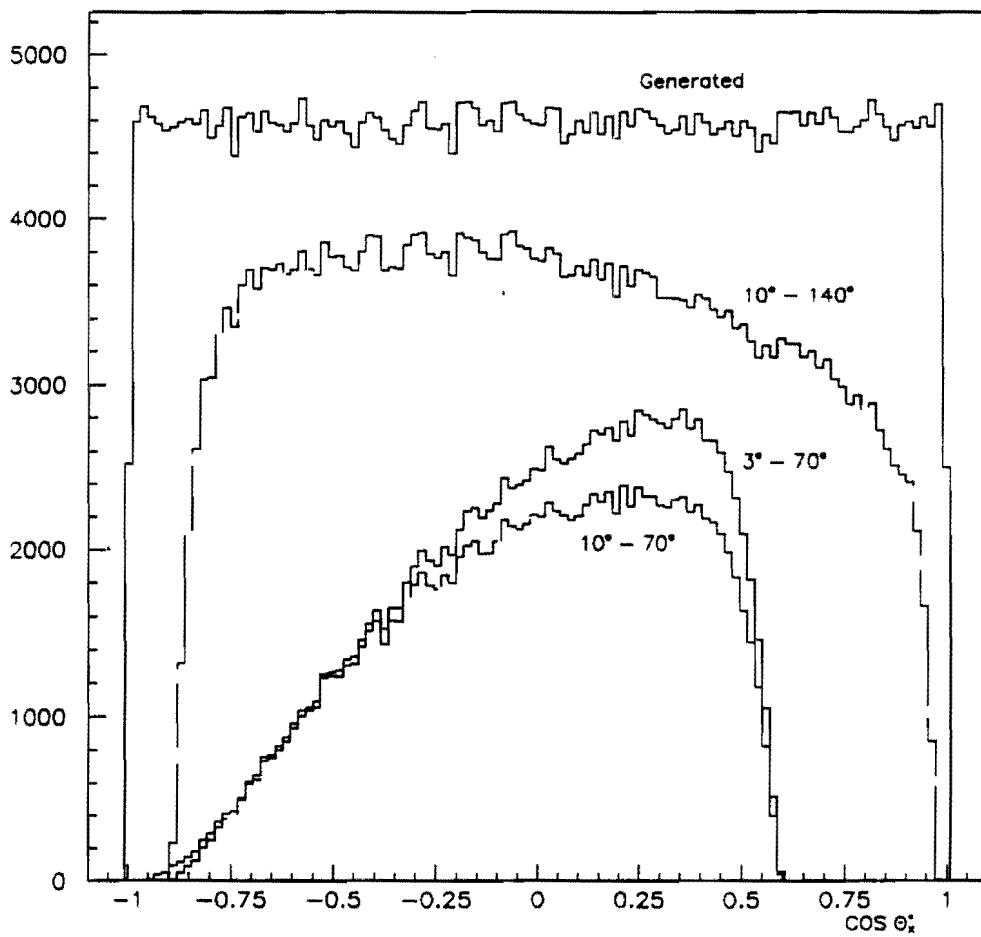


Fig. 6 Acceptance for a  $1.5 \text{ GeV}/c^2$  object decaying to  $\pi^0\pi^0$

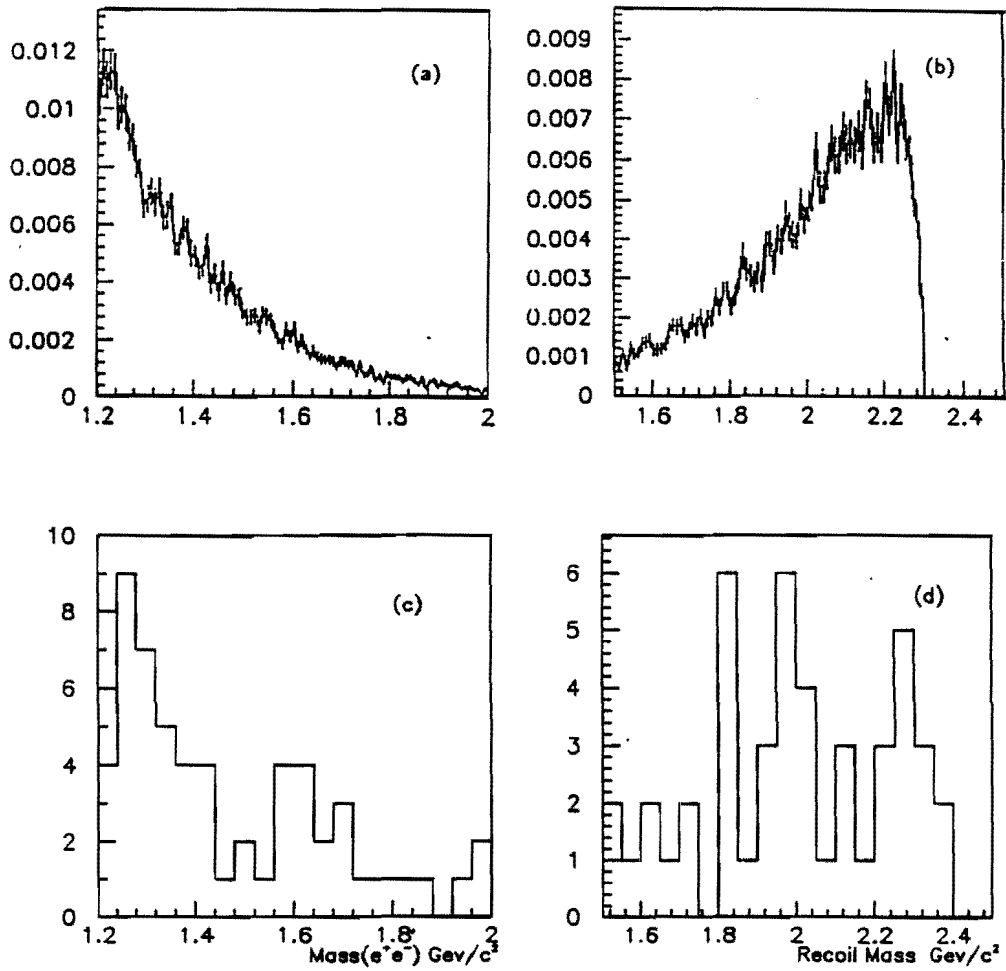
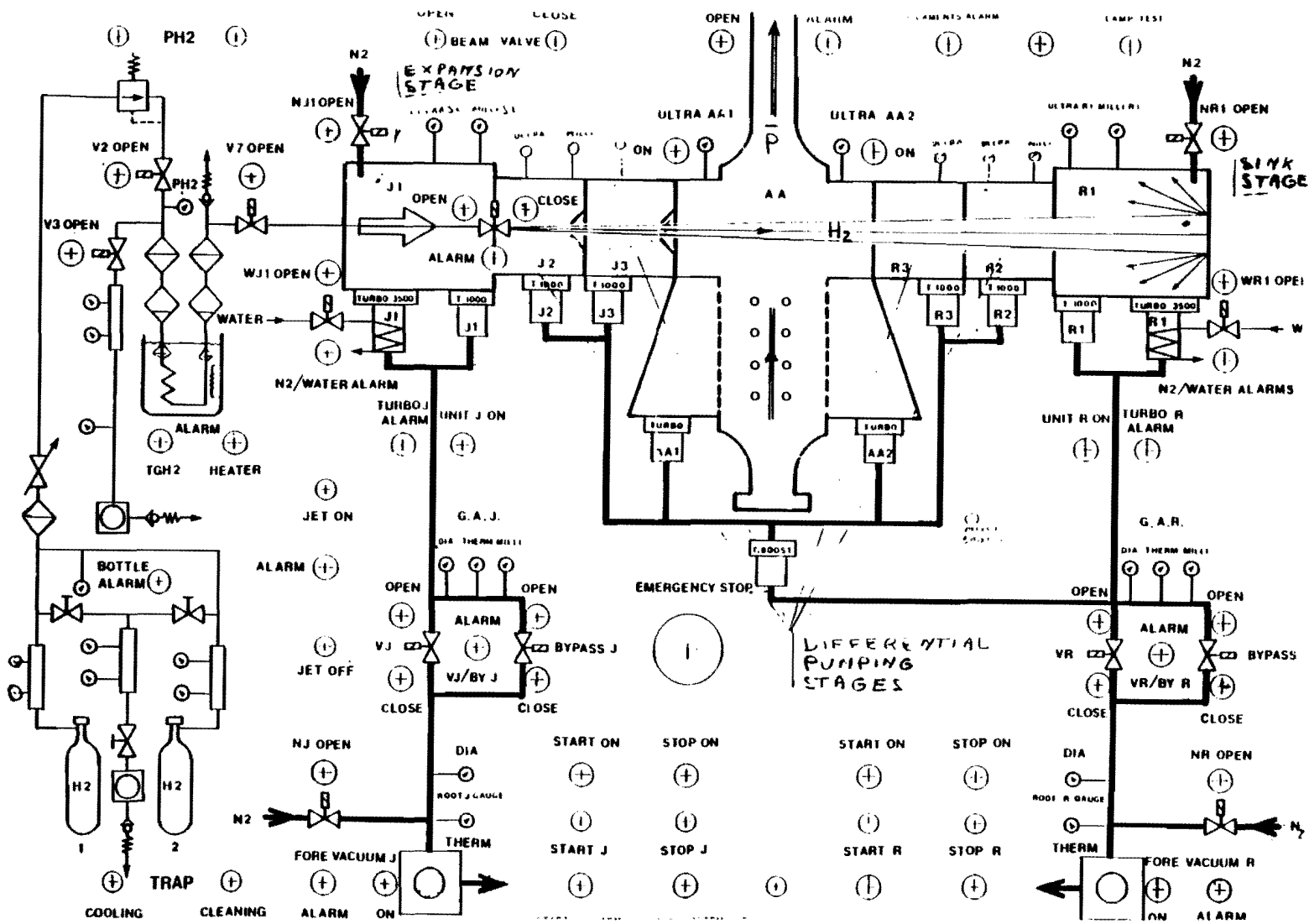
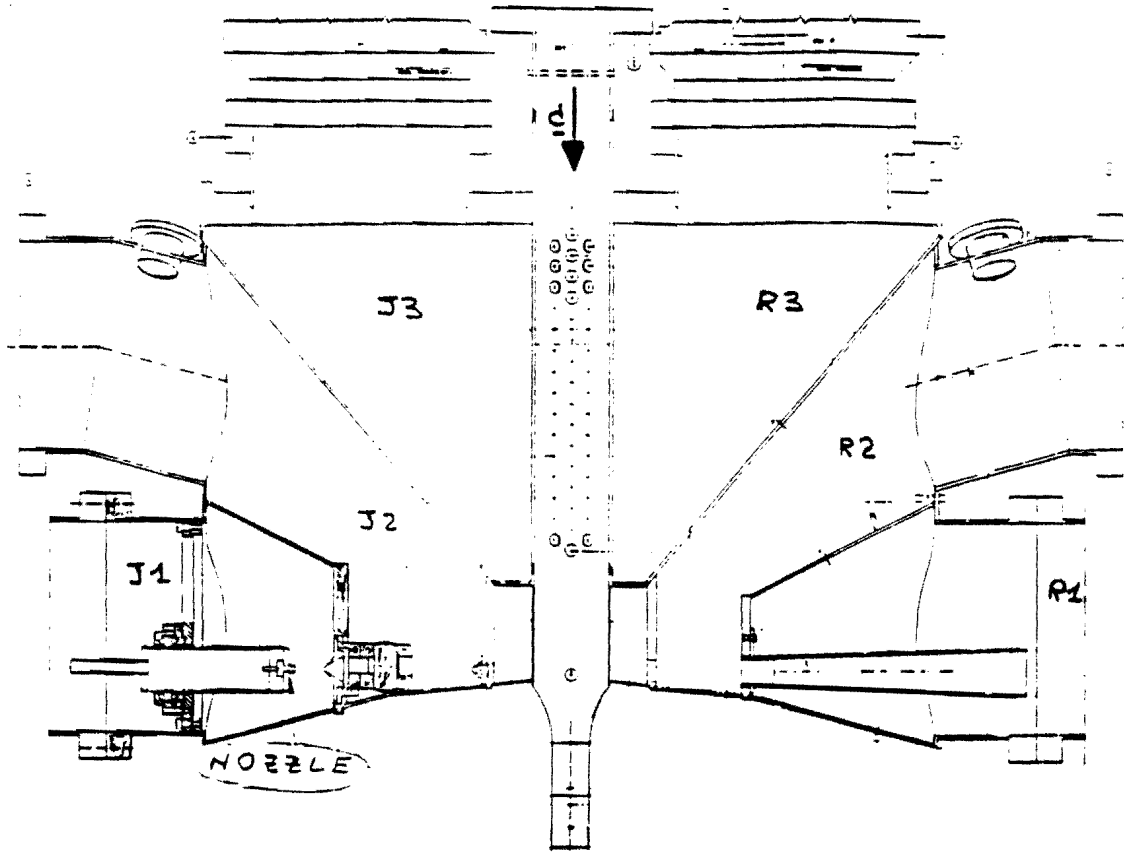


Fig. 7 Drell-Yan production of 4-quark states

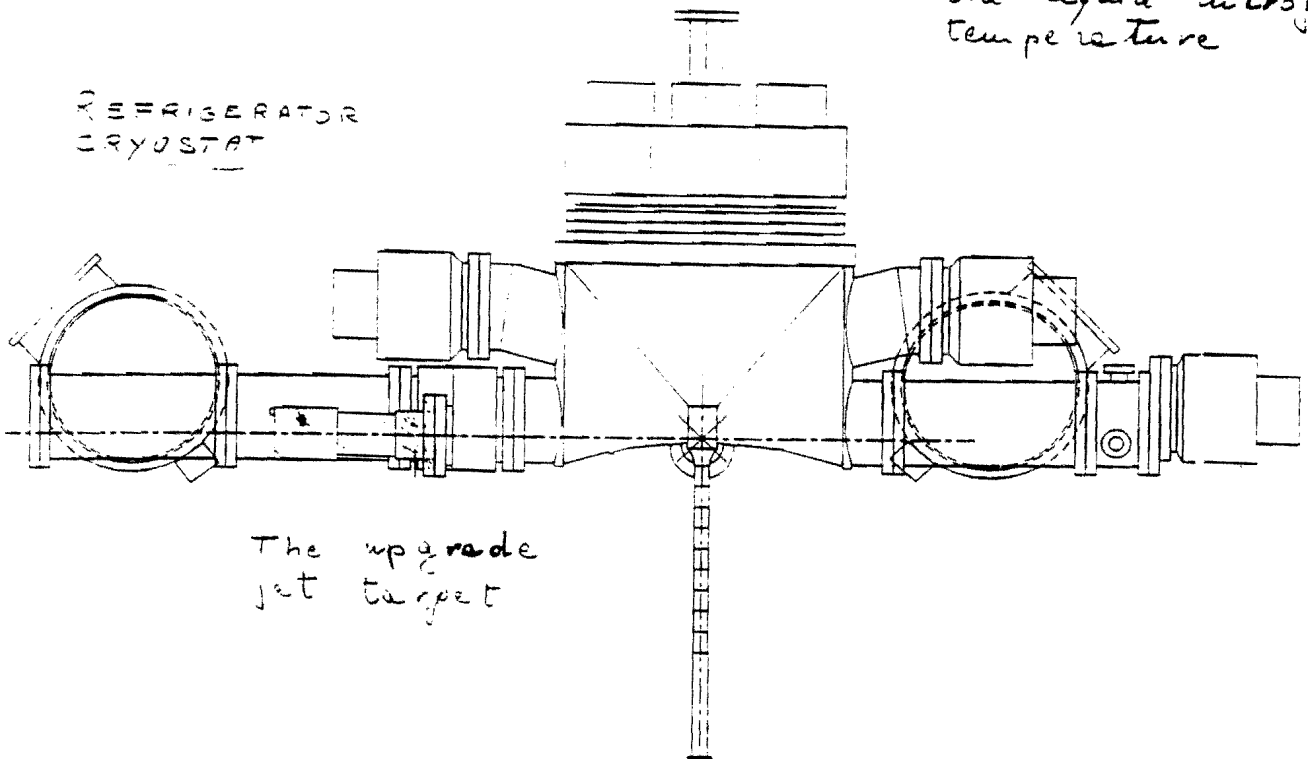
Fig. 8 The E-760 Gas-Jet Target General Schematic





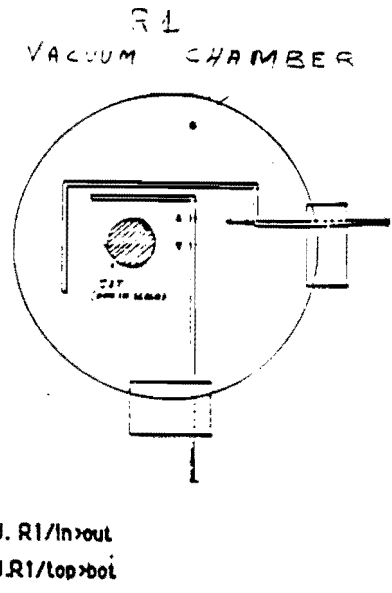
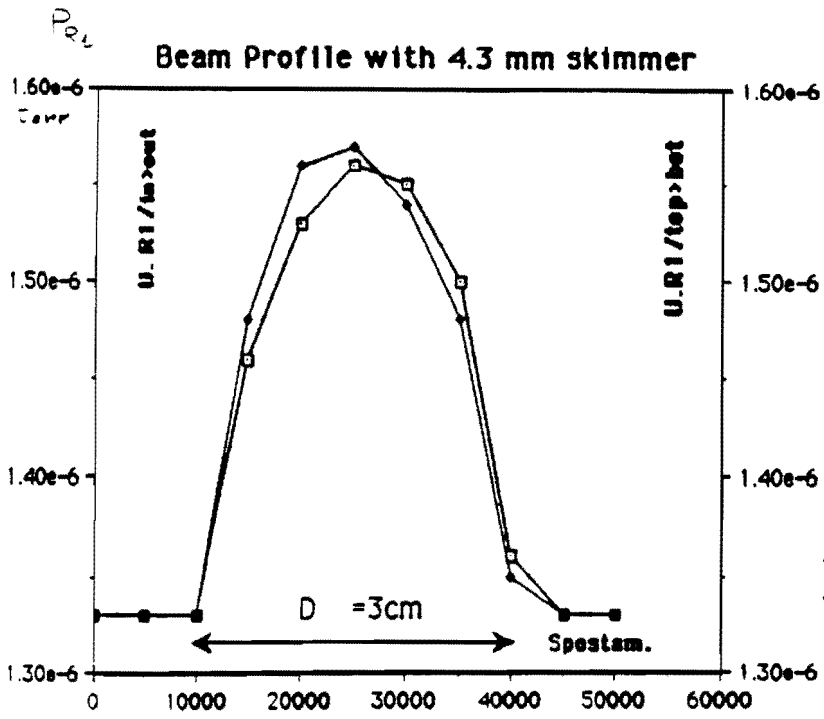
- The jet target with the nozzle at the liquid nitrogen temperature

REFRIGERATOR  
CRYOSTAT

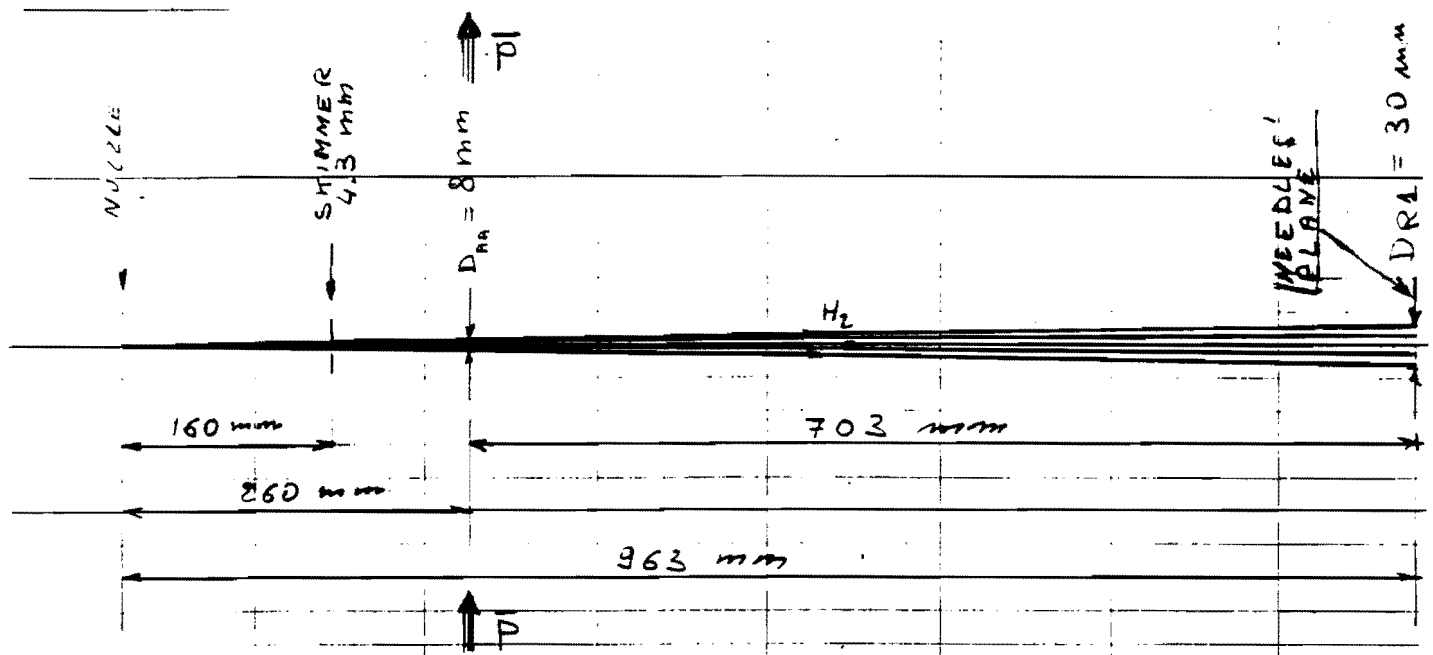


The upgrade jet target

Fig. 9 The E-760 Gas-Jet Target Nozzle Schematic



- increase of the pressure inside the R1 chamber when the needle at the room temperature, cuts the cluster beam.



The cluster beam diameter ( $D_{aq} = 8\text{ mm}$ ) at the crossing point with  $\bar{p}$  beam

Fig. 10 The E-760 Gas-Jet Geometry

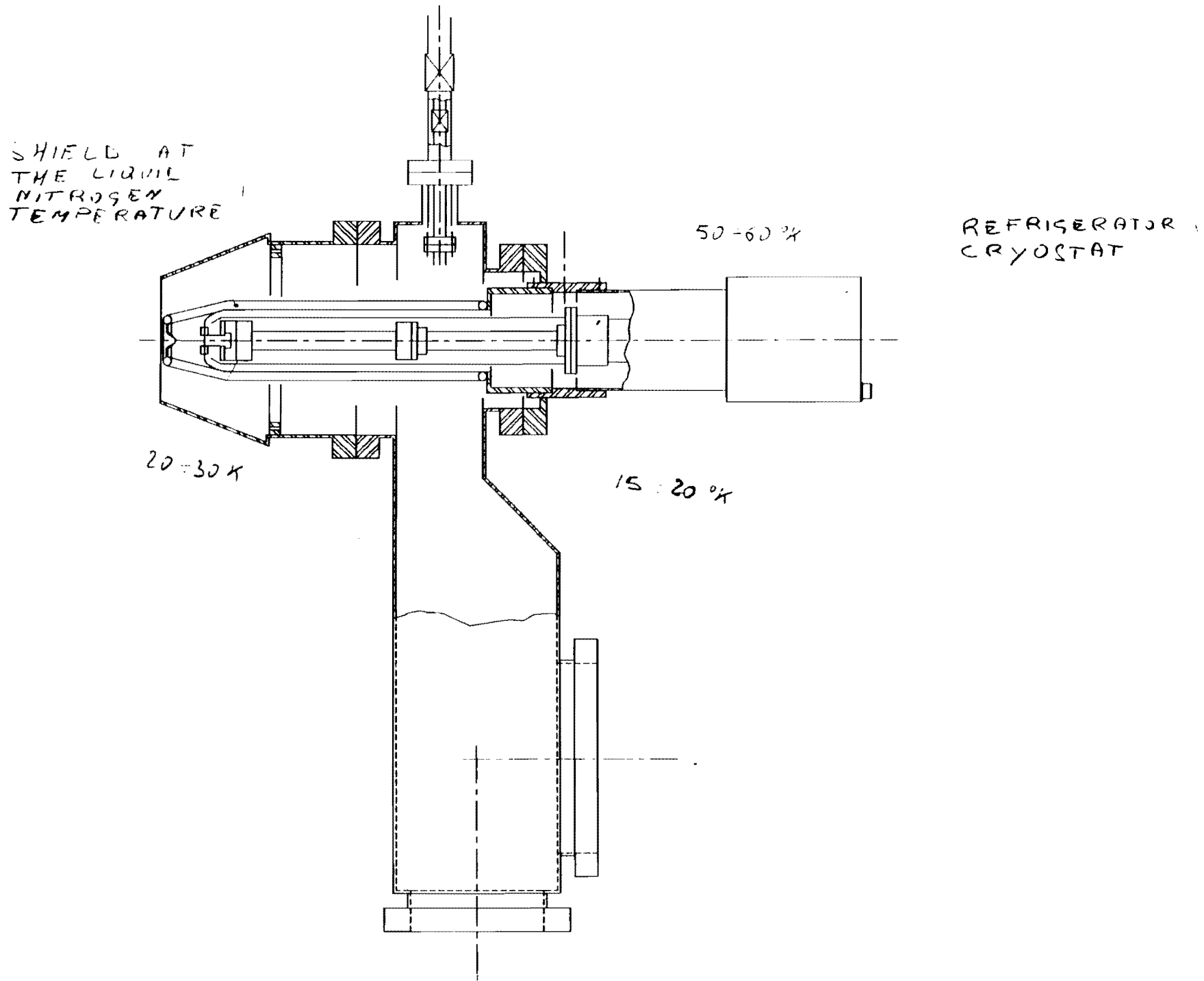


Fig. 11 The P-835 Gas-jet Expansion stage Schematic

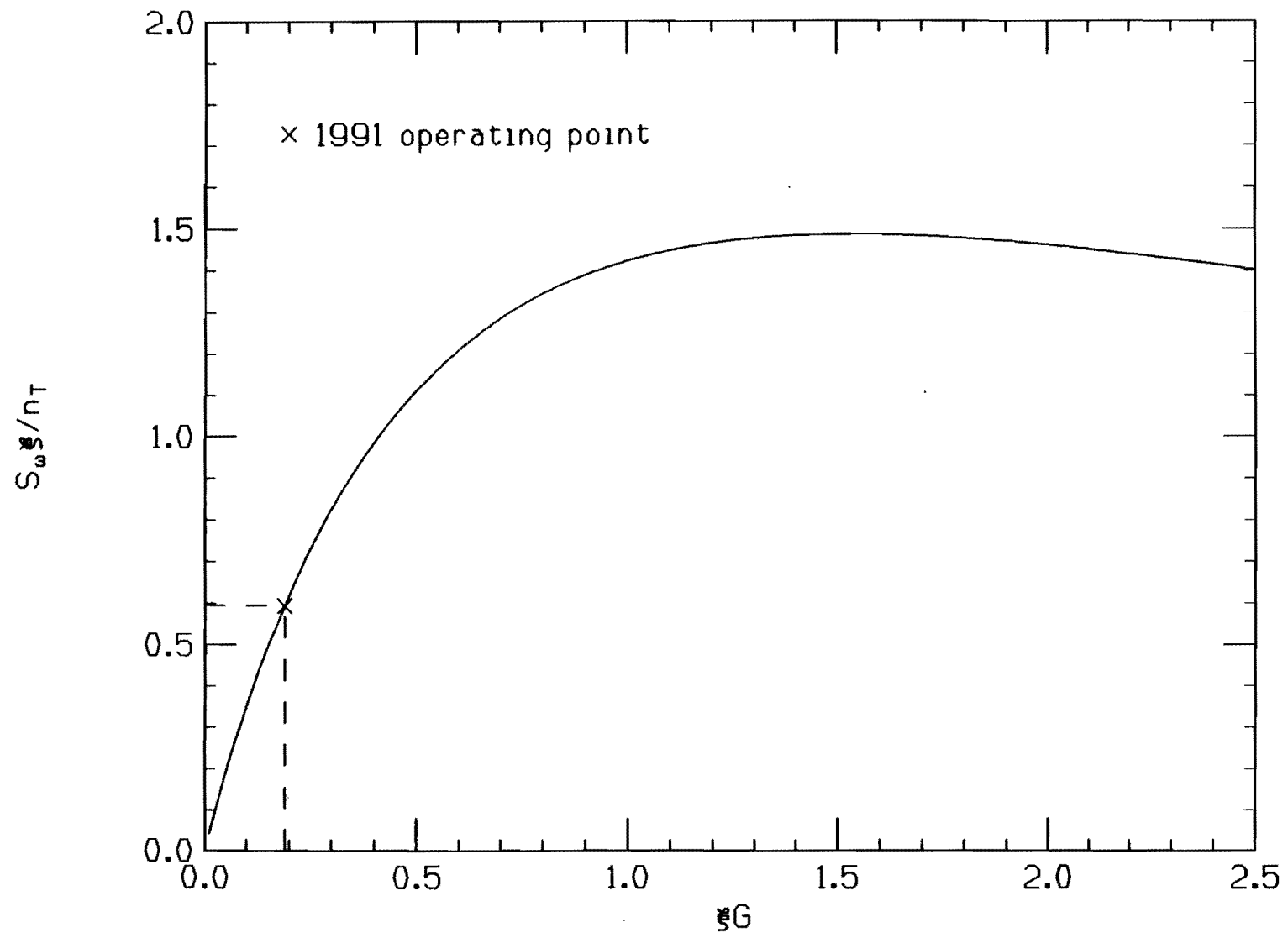
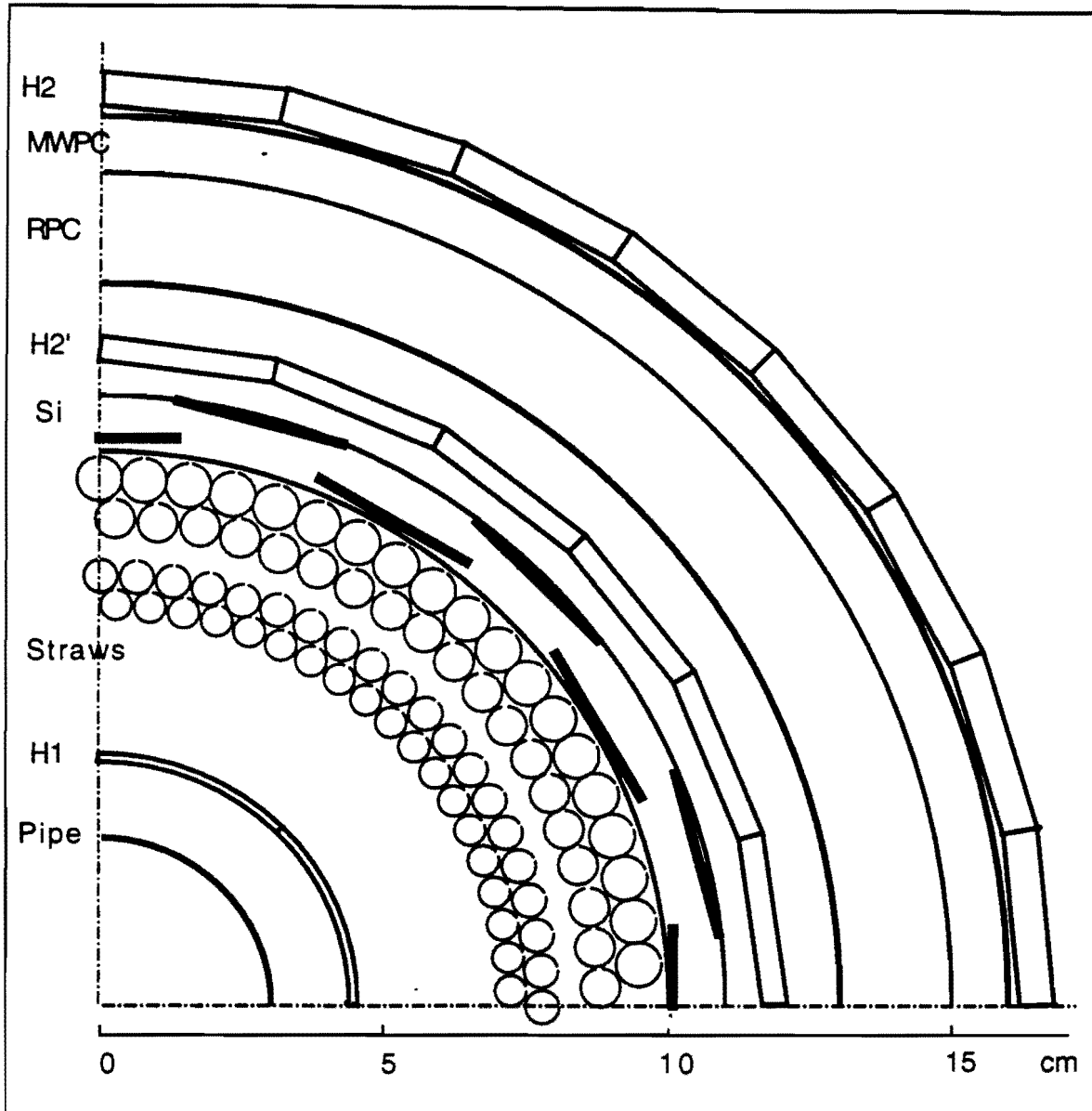


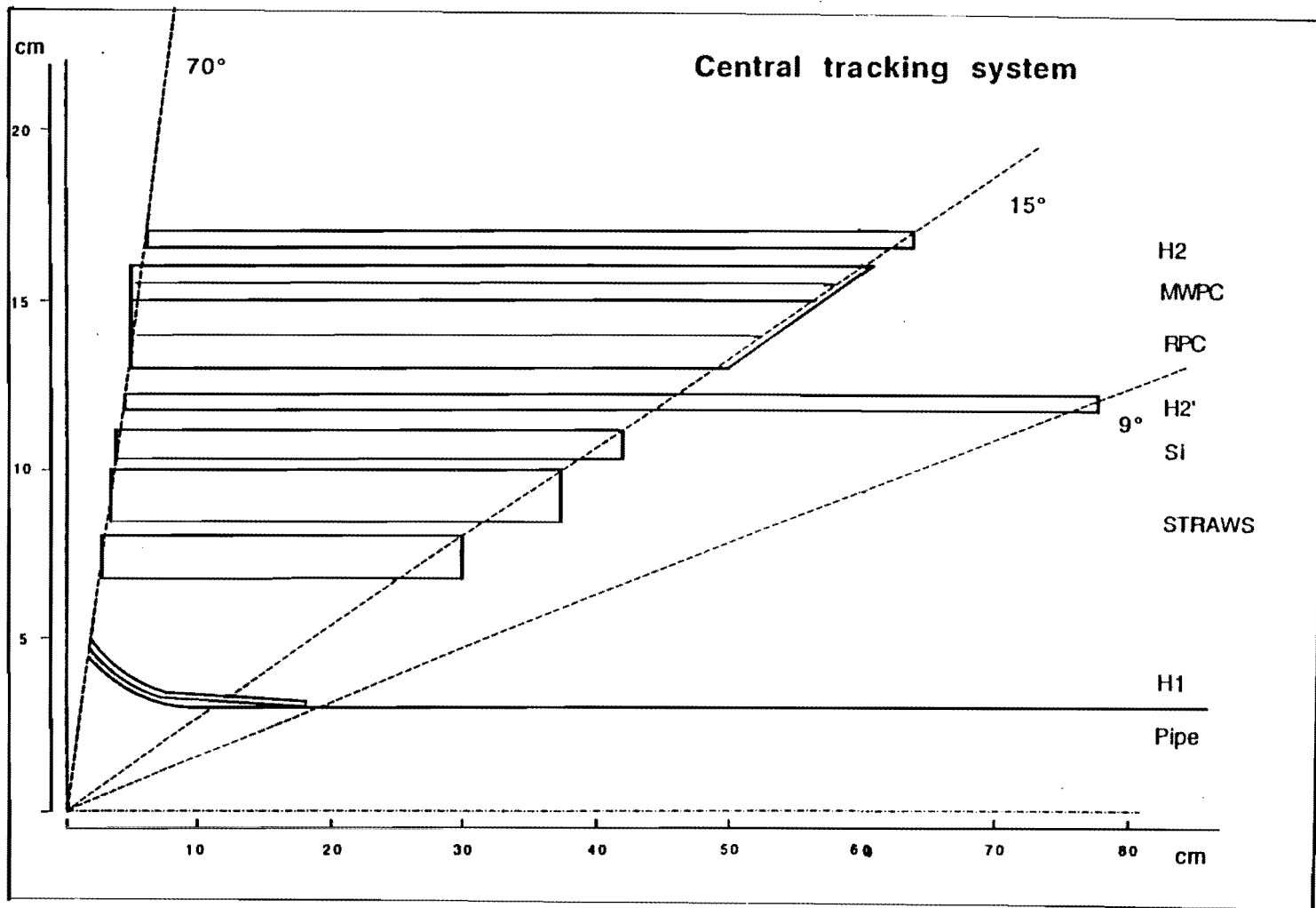
Fig. 12 Antiproton Cooling Rate Parameter Plot



Central tracking detector

Fig. 13 A 90° azimuthal section of the P-835 tracking system

Fig. 14 A longitudinal view of the P-835 tracking system



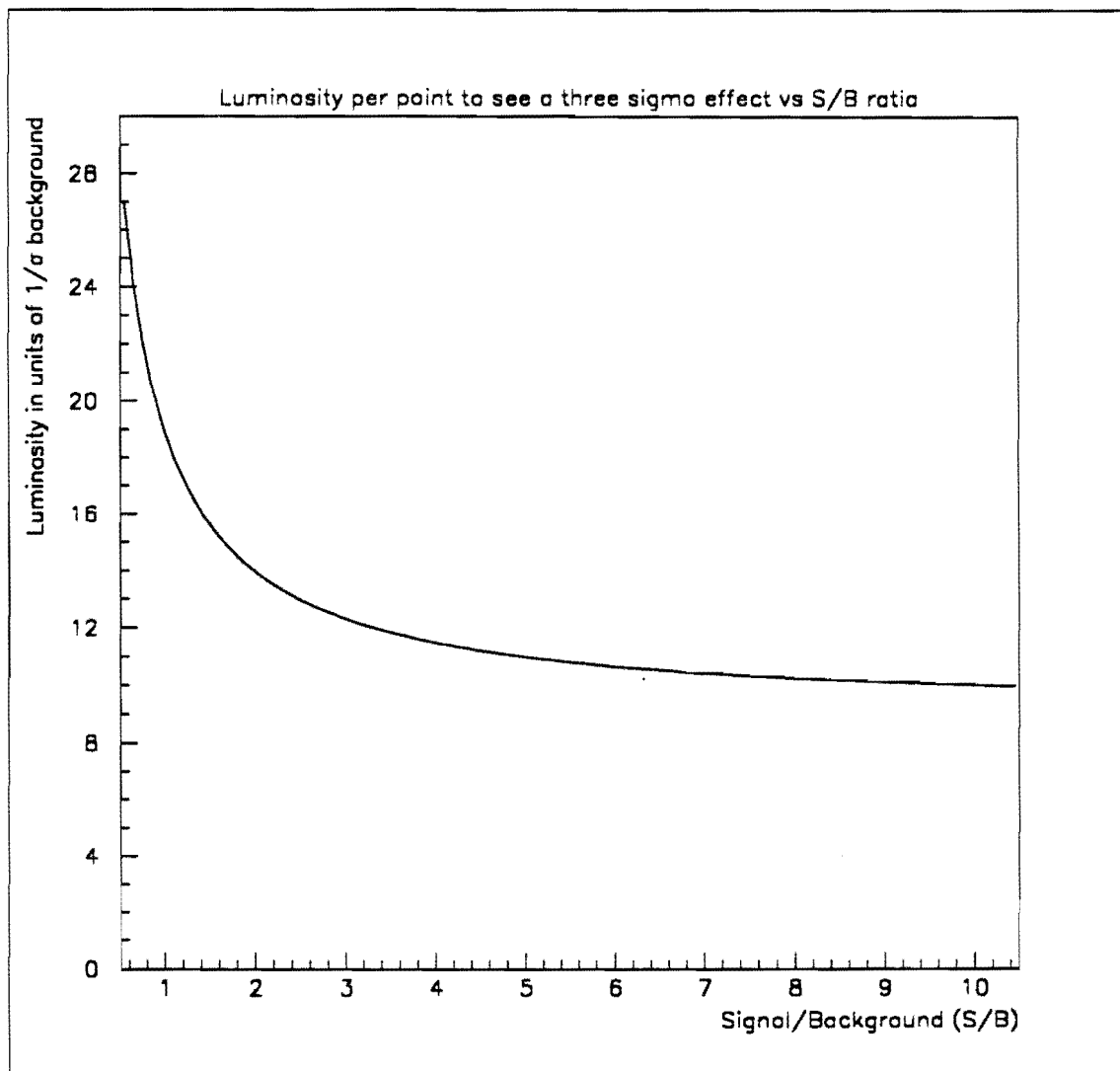


**Fig 15** The luminosity per point needed in an energy scan to see a  $3\sigma$  effect as a function of Signal/Background

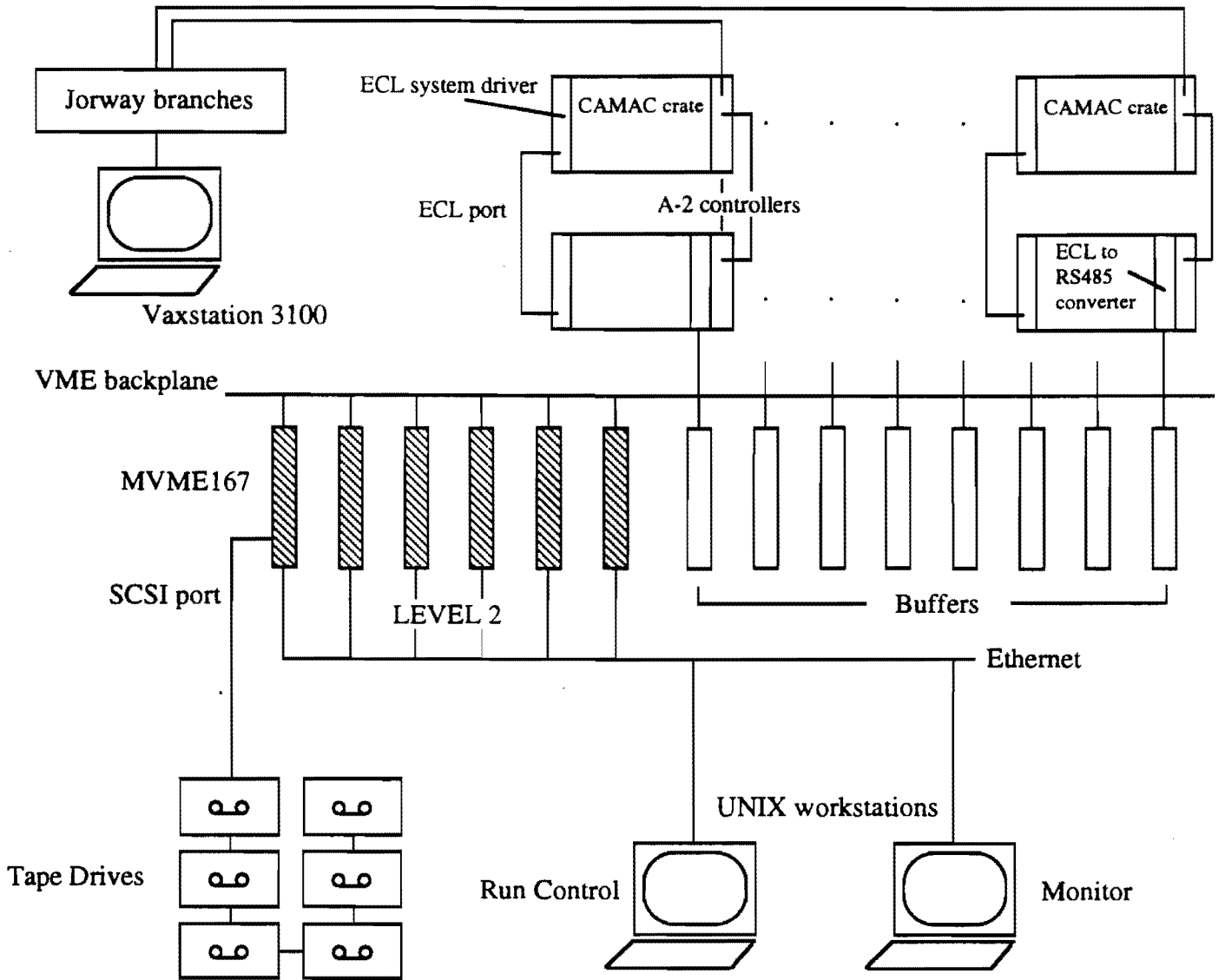


Fig. 16 The P-835 Data Acquisition Scheme

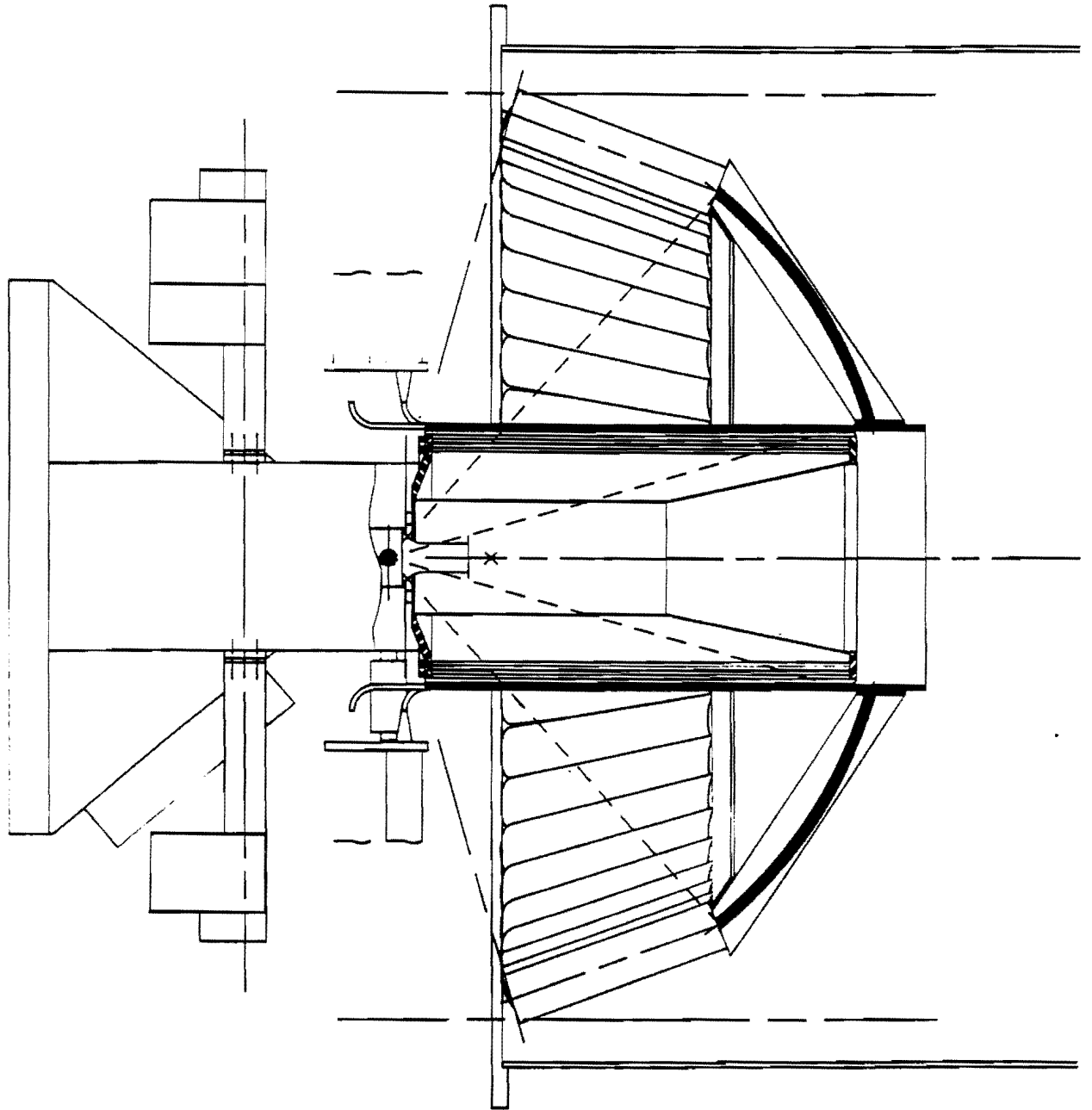


Fig. 17 Schematic of the Fitch Counter